



UNIVERSITY OF LEEDS

This is a repository copy of *Synthesizing multi-sensor, multi-satellite, multi-decadal datasets for global volcano monitoring*.

White Rose Research Online URL for this paper:
<http://eprints.whiterose.ac.uk/137086/>

Version: Accepted Version

Article:

Furtney, MA, Pritchard, ME, Biggs, J et al. (5 more authors) (2018) Synthesizing multi-sensor, multi-satellite, multi-decadal datasets for global volcano monitoring. *Journal of Volcanology and Geothermal Research*, 365. pp. 38-56. ISSN 0377-0273

<https://doi.org/10.1016/j.jvolgeores.2018.10.002>

© 2018 Published by Elsevier B.V. This manuscript version is made available under the CC-BY-NC-ND 4.0 license <http://creativecommons.org/licenses/by-nc-nd/4.0/>.

Reuse

This article is distributed under the terms of the Creative Commons Attribution-NonCommercial-NoDerivs (CC BY-NC-ND) licence. This licence only allows you to download this work and share it with others as long as you credit the authors, but you can't change the article in any way or use it commercially. More information and the full terms of the licence here: <https://creativecommons.org/licenses/>

Takedown

If you consider content in White Rose Research Online to be in breach of UK law, please notify us by emailing eprints@whiterose.ac.uk including the URL of the record and the reason for the withdrawal request.

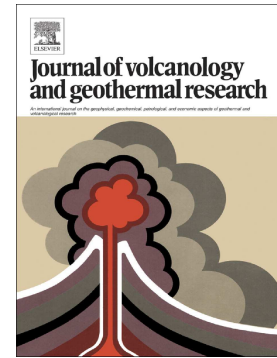


eprints@whiterose.ac.uk
<https://eprints.whiterose.ac.uk/>

Accepted Manuscript

Synthesizing multi-sensor, multi-satellite, multi-decadal datasets for global volcano monitoring

Maria A. Furtney, Matthew E. Pritchard, Juliet Biggs, Simon A. Carn, Susanna K. Ebmeier, Jennifer A. Jay, Brendan T. McCormick Kilbride, Kevin A. Reath



PII: S0377-0273(18)30219-1
DOI: [doi:10.1016/j.jvolgeores.2018.10.002](https://doi.org/10.1016/j.jvolgeores.2018.10.002)
Reference: VOLGEO 6457

To appear in: *Journal of Volcanology and Geothermal Research*

Received date: 6 June 2018
Revised date: 3 October 2018
Accepted date: 3 October 2018

Please cite this article as: Maria A. Furtney, Matthew E. Pritchard, Juliet Biggs, Simon A. Carn, Susanna K. Ebmeier, Jennifer A. Jay, Brendan T. McCormick Kilbride, Kevin A. Reath , Synthesizing multi-sensor, multi-satellite, multi-decadal datasets for global volcano monitoring. *Volgeo* (2018), doi:[10.1016/j.jvolgeores.2018.10.002](https://doi.org/10.1016/j.jvolgeores.2018.10.002)

This is a PDF file of an unedited manuscript that has been accepted for publication. As a service to our customers we are providing this early version of the manuscript. The manuscript will undergo copyediting, typesetting, and review of the resulting proof before it is published in its final form. Please note that during the production process errors may be discovered which could affect the content, and all legal disclaimers that apply to the journal pertain.

Synthesizing multi-sensor, multi-satellite, multi-decadal datasets for global volcano monitoring

Maria A. Furtney^{1,2}, Matthew E. Pritchard¹, Juliet Biggs³, Simon A. Carn⁴, Susanna K. Ebmeier⁵, Jennifer A. Jay^{6*}, Brendan T. McCormick Kilbride⁷, Kevin A. Reath¹

¹ Department of Earth and Atmospheric Science, Cornell University, Ithaca, NY, USA

² Department of Earth, Environmental and Planetary Sciences, Rice University, Houston, TX, USA

³ Centre for the Observation and Modelling of Earthquakes and Tectonics, School of Earth Sciences, University of Bristol, Bristol BS8 1RJ, UK

⁴ Department of Geological Engineering and Sciences, Michigan Technological University, Houghton, MI, USA

⁵ School of Earth & Environment, University of Leeds, LS2 9JT, UK

⁶ Global Volcanism Program, National Museum of Natural History, Smithsonian Institution, Washington D.C., USA

⁷ COMET, Department of Earth Sciences, University of Cambridge, Cambridge, CB2UK

*Now at 2920 Amberleigh Way, Fairfax, VA 22031, USA

Abstract

Owing to practical limitations less than half of Earth's 1400 subaerial volcanoes have no ground monitoring and few are monitored consistently. Earth-observing satellite missions provide global and frequent measurements of volcanic activity that are closing these gaps in coverage. We compare databases of global, satellite-detections of ground deformation (1992-2016), SO₂ emissions (1978-2016), and thermal features (2000-2016) that together include 306 volcanoes. Each database has limitations in terms of spatial and temporal resolution but each technique contributed 45-86 unique detections of activity that were not detected by other techniques. Integration of these three databases shows that satellites detected $\sim 10^2$ volcanic activities per year before the year 2000 and $\sim 10^3$ activities per year after the year 2000. We find that most of the 54 erupting volcanoes without satellite-detections are associated with low volcano explosivity index eruptions and note that many of these eruptions (71%, 97/135) occurred in the earliest decades of remote sensing (pre-2000) when detection thresholds were high. From 1978-2016 we conduct a preliminary analysis of the timing between the onset of satellite-detections of deformation (N=154 episodes, N=71 volcanoes), thermal features (N=16544 episodes, N=99 volcanoes), and SO₂ emissions (N=1495 episodes, N=116 volcanoes) to eruption start dates. We analyze these data in two ways: first, including all satellite-detected volcanic activities associated

with an eruption; and second, by considering only the first satellite-detected activity related to eruption. In both scenarios, we find that deformation is dominantly pre-eruptive (47% and 57%) whereas available databases of thermal features and SO₂ emissions utilizing mainly low-resolution sensors are dominantly co-eruptive (88% and 76% for thermal features, 97% and 96% for SO₂ emissions).

Keywords: Global volcano monitoring, multi-sensor, satellite-detected volcanic activity, deformation, thermal feature, SO₂ degassing

1. Introduction

Though there are over 800 million people living within 100 km of a Holocene volcano – volcanoes that have been active in the past 10,000 years – (Brown et al., 2015a), current estimates suggest that up to 45% of Holocene volcanoes are not monitored, seismically or otherwise (Brown et al., 2015b), and less than 10% are monitored habitually (Ferrucci et al., 2012). Ranking systems have been designed to prioritize volcanic threat and optimize monitoring strategies at frequently “active” volcanoes (e.g. Ewert, 2007; Barberi, 1990) though some of the most devastating eruptions occur after very long intervals of quiescence (100s of years, e.g. Chaiten: S.F.L. Watt et al., 2013; Carn et al., 2009b, Lara, 2009; Pinatubo: McCormick et al., 1995, Bluth et al., 1992). Additionally, numerous examples in the literature demonstrate that Holocene volcanoes are not the only volcanoes that are restless (e.g. Francis and De Silva, 1989; Pritchard and Simons, 2004; Lu and Dzurisin, 2014; Pritchard et al., 2014), and therefore monitoring certain Pleistocene and older volcanoes is also needed.

Vigilant monitoring is one requisite to provide earliest warning of volcanic catastrophes, yet constant monitoring of all potentially active volcanoes (*sensu lato*) would be challenging both logistically and economically (e.g. Brown et al., 2015b). Here is where a global integration of multi-sensor satellite data can offer assistance. Satellite observations have provided critical

data for remote and inaccessible volcanoes (e.g. Harris et al., 1999; Dean et al., 2002; Goitom et al., 2015), and satellite imagery can survey areas 100s of kilometers wide, providing complete coverage of volcanic regions (e.g. Francis and De Silva, 1989; Pritchard and Simons, 2002; Carn et al., 2003; McCormick et al., 2012; Henderson and Pritchard, 2013). Ground deformation, gas output, and thermal features can be resolved through the use of specific sensors deployed on satellites (e.g. Pritchard and Simons, 2002; McCormick et al., 2012; Jay et al., 2013; Bignami et al., 2014), thus aiding the identification of active areas where greater attention and the deployment of ground-based instrumentation may be warranted (e.g. Philibosian and Simons, 2011).

The global coverage of the multi-sensor satellite approach supplements the historically-dominated ground-based measurements of volcanic unrest. With more comprehensive datasets of volcanic activity chronology it will become easier to define repose times. Compiled datasets of ground-based observations have been used for this purpose (e.g. Phillipson et al., (2013) and Passarelli and Brodsky (2012)), yet a similar analysis has not yet been undertaken for satellite datasets. Here, we compile global databases of satellite-detections and delineate their time of measurement relative to eruptions to compare against similar ground-based studies (Phillipson et al. (2013) and Passarelli and Brodsky (2012)). Our global databases involve satellite-detections from three methods: volcanic deformation from synthetic aperture radar (SAR), thermal features from thermal infrared (TIR), and SO₂ degassing from ultraviolet (UV) spectroscopy. Our time series starts in 1978 with just the UV technique, but as additional satellites have been launched we are currently approaching global coverage from all three techniques. Other types of satellite sensors have detected volcanic activities (for example, degassing observations from TIR spectroscopy) but are not considered here. Importantly, we define the term “satellite-detected

volcanic activity” somewhat broadly to describe any satellite-detection at a volcano without regard for its relation to eruption to avoid bias in our analysis. Thus, satellite-detections catalogued in our database may originate before an eruption, during an eruption, or may occur without any eruption.

This global synthesis of volcanic activity detected by three different types of satellite sensors is the first study of its kind. Our methods are largely exploratory to determine the potential of this multi-satellite, multi-sensor, multi-decadal perspective to contribute to global volcano monitoring strategies, demonstrate preliminary patterns in global volcanic satellite-detections and global volcano risk, and identify monitoring gaps. We explore pressing volcanology questions about the commonness or uniqueness of volcanic activity (e.g. Cashman and Biggs, 2014) by associating volcanoes that produce similar types of activity (deformation, thermal features, SO₂ degassing) prior to eruption, though do not comment on the magnitude of these activities. We also aim to quantify the time periods between satellite-detections of volcanic activity and eruption to determine which type of detection may provide the earliest indication of impending eruption. Studies using ground-based data suggest that deformation is the earliest precursor (e.g. Phillipson et al., 2013), and we test whether this is additionally true from satellite data that includes different detection thresholds and biases. Finally, we highlight recommendations for a global satellite monitoring system and describe the limits of satellite observations and ground-based methods.

2. Methods

We have assembled satellite-detections of volcanic activities from three types of sensors which include many generations of satellites, sensors, and the integration of multi-decadal

databases. Yet our catalogues are incomplete owing to insufficient resolutions, repeat intervals, and detection thresholds of available satellite systems that limit their ability to detect volcanic activity under certain circumstances. Additional limitations arise from conditions of the atmosphere as the propagating medium, data processing method, and emitted wavelength or spectral range of the sensor. Since the average satellite lifespan is on the order of a decade, multiple satellite records must be assembled to form a long-term dataset. As a result, resolutions and detection thresholds change with time (see Table 1) and our database is not continuous through time or space.

Further, our database is dominated by observations of subaerial Holocene volcanoes included in the Global Volcanism Program Volcanoes of the World database (2013, <https://volcano.si.edu/>) with associated volcano identification numbers. We additionally include seven volcanoes described in section 2.1 that did not have associated volcano identification numbers, either because they are older than Holocene or are listed inclusively with other volcanic edifices. For example, the late-Pliocene to early Pleistocene volcano Hualca Hualca (Peru) is not listed individually in the Global Volcanism Program Volcanoes of the World database though is mentioned on the page for the nearby Holocene volcano Sabancaya (Peru). A deformation survey by Pritchard and Simons (2002) measured a deformation source in closer proximity to Hualca Hualca (2.5 km) than to Sabancaya (7 km), so we associate the deformation with both Hualca Hualca and Sabancaya. Given that volcano names and precise locations are variable throughout the literature, we use the volcano numbers to compare across the four categories: deformation, thermal features, SO₂ degassing, and eruption, and assign new numbers to the seven volcanoes not listed by the Global Volcanism Program.

For each type of activity: deformation, thermal, SO₂ degassing, and eruptions, we create

Instrument	Method	Sensor range	Nadir footprint	Repeat interval	Detection threshold	Life span	References
ERS-1,2	SAR	C-band, 5.66 (cm)	26x6 (m)	35 (days)	1 (cm, single interferogram) or 2-3 (mm/yr, from timeseries)	1991-2000	Massonnet and Feigl, 1998; Pyle et al., 2013; Ebmeier et al., 2018
JERS-1	SAR	L-band, 23.5 (cm)	18x6 (m)	44 (days)	1 (cm, single interferogram) or 2-3 (mm/yr, from timeseries)	1992-1996	Massonnet and Feigl, 1998; Pyle et al., 2013; Ebmeier et al., 2018
RADARSAT-1,2	SAR	C-band, 5.6 (cm)	5x8, 25x28, 100 (m)	24 (days)	1 (cm, single interferogram) or 2-3 (mm/yr, from timeseries) (cm)	1995-2013	Massonnet and Feigl, 1998; Pyle et al., 2013; Ebmeier et al., 2018
Envisat	SAR	C-band, 5.6 (cm)	30x30, 150x150 (m)	35 (days)	1 (cm, single interferogram) or 2-3 (mm/yr, from timeseries) (cm)	2002-2012	Pyle et al., 2013; Ebmeier et al., 2018
ALOS-1	SAR	L-band, 23.5 (cm)	10, 100 (m)	46 (days)	2-3 (cm/yr from timeseries)	2006-2011	Semple et al., 2017; Chaussard et al., 2014; Pyle et al., 2013; Ebmeier et al., 2018
ALOS-2	SAR	L-band, 23.5 (cm)	3, 60 (m)	14 (days)	2 (cm/yr from timeseries)	2014-present	Fujiwara et al., 2017; Pyle et al., 2013; Ebmeier et al., 2018
COSMO-SkyMed-1,2,3,4	SAR	X-band, 3.1 (cm)	1, 3-5, 30 (m)	16 (days, ≥ 1 for full constellation)	1 (cm, single interferogram) or 2-3 (mm/yr, from timeseries)	2007-present	Pyle et al., 2013; Ebmeier et al., 2018
TerraSAR-X,TanDEM-X	SAR	X-band, 3.1 (cm)	0.25, 3, 40 (m)	11 (days)	1 (cm, single interferogram) or 2-3 (mm/yr, from timeseries)	2007-present	Pyle et al., 2013; Ebmeier et al., 2018
Sentinel-1a,1b	SAR	C-band, 5.6 (cm)	5x5, 5x20, 25x100 (m)	12 (days, 6 for 1b)	1 (cm, single interferogram) or 2-3 (mm/yr, from timeseries)	2014-present	Pyle et al., 2013; Ebmeier et al., 2018
Nimbus-7 TOMS	UV/VIS	300-340 (nm)	50 (km)	1 (day)	10700 (t)	1978-1993	Carn et al., 2003
Meteor-3 TOMS	UV/VIS	300-340 (nm)	62 (km)	1 (day)	16460 (t)	1991-1994	Carn et al., 2003
Earth Probe TOMS	UV/VIS	300-340 (nm)	39x39 (km)	1 (day)	1440-3800 (t)	1996-2002	Carn et al., 2003
ADEOS TOMS	UV	300-340 (nm)	42 (km)	1 (day)	3780 (t)	1996-1997	Carn et al., 2003
OMI	UV/VIS	270-500 (nm)	24x13 (km)	1 (day)	26 (t)	2004-present	McCormick et al., 2013
MODIS	TIR	3.959 (μm , Band 21 or 22) and 12.02 (μm , Band 32)	1 (km)	0.5 (days, twice per day for each Terra and Aqua satellites)	Variable (for MODVOLC algorithm, the NTI threshold is ≥ -0.8 for night and ≥ -0.6 for day)	1999-present	Wright et al., 2014; Zaksek et al., 2013; Wright et al., 2004; Wright et al., 2002
ASTER	TIR	8.125-11.65 μm	90 (m)	16 (days at the equator, ≥ 1 day for Urgent Request Protocol)	$\geq 1.5\text{K}$ above background	1999-present	Ramsey, 2015; Abrams et al., 2004; Pieri and Abrams, 2004; Ramsey and Dehn, 2004; Wright et al., 1999; Gillespie et al., 1998; Yamaguchi et al., 1998

Table 1. Sensor information and detection thresholds (under optimal conditions) for instruments used in our databases. The OMI and TOMS detection limits are calculated for a cluster of 5 nadir pixels at 5σ (where 1σ is defined as the standard deviation from the combined noise due to the instrument, measurement, retrieval, and random errors). The NTI threshold is shorthand for the Normalized Thermal Index, a ratio of the difference of the spectral radiance emitted by a surface in the middle infrared versus longwave infrared divided by their sum.

two databases: one for a spatial analysis and one for a timing analysis. The spatial databases include the names of volcanoes where satellite-detected activities have been recorded. The timing database includes the names of volcanoes where satellite-detected activities have been recorded as well as the time the satellite-detected activities were recorded. The following sections describe in more detail each of the satellite sensors used in our analysis and how we compiled our databases.

2.1 Thermal infrared (TIR) database

2.1.1 TIR data

Although the earliest generations of satellite thermal sensors (i.e. High-Resolution Infrared Radiometer (1964-1974), Advanced Very High Resolution Radiometer (1978-present), and the Landsat Thematic Mapper (1982-present)) were not specifically designed with volcano monitoring in mind, their observations fueled significant strides in studies of volcanic eruptions and thermal features (e.g. Bonneville et al., 1985; Bonneville and Kerr, 1987; Francis and Rothery, 1987; Rothery et al., 1988). Here we focus on thermal infrared data from the Advanced Spaceborne Thermal Emission and Reflection Radiometer (ASTER) and the MODVOLC algorithm derived from the Moderate Resolution Imaging Spectroradiometer (MODIS). Both are aboard the Terra (1999-present) and Aqua satellites (2002-present) and have been used to track volcanic eruptions (e.g. Nye et al., 2002; Delgado et al., 2014), in thermal feature detection (e.g. Patrick and Smellie, 2013), and to identify eruptions from volcanoes without prior activity (e.g. Wright et al., 2004). The instrument details for ASTER and MODIS, including lifespans, sensor specifications, resolutions, and detection thresholds, are available in Table 1.

For detection of volcanic thermal features from MODIS data we primarily use the automated MODVOLC algorithm developed at the University of Hawai'i's Institute of Geophysics and Planetology. (For more information, the reader is referred to Wright et al., 2002; and Wright et al., 2004). A threshold for the normalized thermal index allows for automated detection of thermal features on a global scale and minimizes false detections (Wright et al., 2004). These data are updated hourly and are readily available online (modis.higp.hawaii.edu).

In addition to MODVOLC there are a handful of currently operational automated monitoring systems for thermal features at volcanoes: The ASTER Volcano Archive of the Jet Propulsion Laboratory, the Volcanic Cloud Monitoring Web Portal of NOAA/CIMSS (that includes weather satellites like GOES; Pavolonis et al., 2016), HOTVOLC of the Observatoire de Physique du Globe de Clermont-Ferrand, and the Middle InfraRed Observation of Volcanic Activity (MIROVA) from the Universities of Turin and Florence. We do not include detections of thermal features from the ASTER Volcano Archive, which is not currently optimized to detect non-eruptive thermal features (e.g. Furtney, 2016). We also do not include detections of thermal features from the Volcanic Cloud Monitoring Web Portal (July 2015-present), HOTVOLC (2010-present), or MIROVA (most recent alerts only) due to the recent development of these sites and short records. We note that MIROVA, like MODVOLC, uses MODIS data yet offers improved detection of volcanic hotspots owing to an enhanced algorithm employing both spectral and spatial analysis (Coppola et al., 2016a; Coppola et al., 2016b). Finally, although Landsat thermal observations have been useful for volcano studies as mentioned previously, we do not include them in our compilation because of the lack of global nighttime coverage.

There are compilations describing yearly volcanic heat flux and thermal output as a function of time (e.g. Wright and Flynn, 2004; Wright and Pilger, 2008; Delle Donne et al.,

2010), and a few describing thermal features at volcanoes measured by MODVOLC (e.g. Wright et al., 2015; Wright, 2016). However, one key issue with TIR sensors and with satellite monitoring in general is the trade-off between spatial and temporal resolution. More frequent satellite passes optimize the detection of short duration thermal features, which is generally only achievable for low spatial resolution sensors. As an example, MODIS data have high temporal resolution (twice daily) but low spatial resolution (about 1x1 km pixel), this favors the detection of larger and hotter thermal features at the expense of subtler thermal features associated with small magnitude eruptions or fumaroles (e.g. Harris, 2013; Jay et al., 2013). We therefore assembled the first global dataset of volcanic thermal features that combines MODIS (globally) and ASTER data (regionally) to provide more complete coverage.

2.1.2 Formation of the volcano TIR database

We downloaded global data from the MODVOLC database (between 2000-2016, included 13,454,594 thermal alerts) and removed daytime detections of thermal features (where the sun zenith is reported as greater than 90 degrees, then 2,243,342 thermal alerts remained) that are heavily influenced by solar reflection and heating and are not reliable (e.g. Wright et al., 2002). Using the remaining nighttime thermal features, we compared distances between thermal features and volcanoes where we suspected we might find thermal features – including all subaerial Holocene volcanoes (Global Volcanism Program, 2013), and an additional seven volcanoes. These extra seven all had reported activity determined from previous deformation surveys: Gabho (Ethiopia: Wright et al., 2006), Haledebi (Ethiopia: Biggs et al., 2011), Ol Doinyo Gelai (Tanzania, not to be confused with Ol Doinyo Lengai: Baer et al., 2008), Hualca Hualca (Peru: Pritchard and Simons, 2002), Sillajhuay (Chile: Pritchard et al., 2014), near Cerro Overo (Chile: Henderson and Pritchard, 2013), and Gjalp (Iceland: Pagli et al., 2007). There are

various definitions of an “active volcano”, including fumarolically active, seismically active, and where an eruption has occurred within the past 10,000 years (e.g. Pritchard and Simons, 2004).

For our purposes, an active volcano is any volcano with a satellite-detection.

We removed all thermal features more than 20 km from active volcanoes (locations provided by the Global Volcanism Program, 2013) using our definition, assuming thermal features outside of this radius to be non-volcanic (84,614 thermal alerts remained). This is not universally true, of course, as volcanoes like Kilauea (United States) produce fissure eruptions greater than 20 km from the summit and this is a limitation of our method. However, a constraint needed to be imposed in order to remove numerous false detections of thermal features, and we note that our database does include thermal alerts for Kilauea. This distance constraint provides a first-order way of associating thermal features with volcanoes and is approximately the maximum distance from a volcano center at which volcanic deformation has been measured (e.g. Lu and Dzurisin, 2014; Ebmeier et al., 2018). Given that deformation is often the result of motion by magmas or geothermal fluids, we assume that a similar radius might be expected for thermal features.

At present, the MODVOLC algorithm is unable to distinguish between volcanic features, fires, and anthropogenic heat sources, therefore our database initially included many false detections. We remedied this in two ways. First, we searched for thermal feature “clusters”, where at least 10 thermally anomalous pixels (above the normalized thermal index) were identified within two km of each other over the entire time window (1999-2016). Next, these thermal clusters were verified with reports of volcanic activity from the Global Volcanism Program (2013) and invalidated if they did not correspond with reported field observations of volcanic activity. Although confirming volcanic activity with the Global Volcanism Program

(2013) biases the data, this step strengthens identification of a true volcanic origin (Wright, 2016). Locations of thermal clusters were also verified with optical imagery (Google Earth) and removed if they coincided with cities, factories, or locations of known fires. Our methodology found MODVOLC thermal features at volcanoes that were identified in similar analyses by Wright et al., (2015) and Wright, (2016), but new activity at six volcanoes was found using our technique: Sangeang Api (Indonesia), Meager (Canada), Alaid (Kuril Islands), Momotombo (Nicaragua), Wolf (Ecuador), and Sinabung (Indonesia). Our thermal database includes 101 volcanoes identified by MODVOLC (total of 53,548 thermal alerts).

We also compiled published regional and global reports of volcanic thermal features detected by MODIS and ASTER sensors: Jay et al., 2013 (survey of Central and Southern Andes between 2000-2010); Delle Donne et al., 2010 (global study between 2000-2006); and Patrick and Smellie, 2013 (survey of Antarctica and Southern Oceans between 2000-2010). This added an additional 45 volcanoes to our thermal detections database, so that our final spatial thermal database includes 146 volcanoes (see supplementary Table 3). For our timing thermal database, we only used the high temporal resolution yet low spatial resolution MODVOLC data (see supplementary text “MODVOLC_hotspot.txt” with 53,222 MODVOLC alerts for 101 volcanoes).

2.2 InSAR database

2.2.1 SAR data

Interferometric synthetic aperture radar (InSAR) utilizes microwaves to measure sub-centimeter displacements of the ground (e.g. Fournier et al., 2010; Massonnet and Feigl, 1998) over areas hundreds of kilometers wide (e.g. Henderson and Pritchard, 2013) which may provide information regarding movement of magma or hydrothermal fluids within the mid to upper crust

(e.g. Lu, 2007). Satellites carrying SAR sensors (~17 civilian missions since 1992 with further missions planned, e.g. Pinel et al., 2014) have been providing global observations of deformation albeit with different satellite lifespans and detection limits (see Table 1 for more information). More recent sensors (e.g. TerraSAR-X and CosmoSkyMed) exhibit high spatial and temporal resolution and have been able to detect transient deformation in the shallow conduit prior to explosive eruptions (e.g. Salzer et al., 2014; Stephens et al., 2017) and quantify deformation magnitudes and spatial extents more accurately than previous generations of sensors could (e.g. Prati et al., 2010; Wang et al., 2018).

The greatest limiting factors in SAR surveys are the lack of data acquired in certain areas and loss of coherence as a function of time, owing to snow coverage or vegetation growth, for example, that cause significant changes to land cover between the acquisition of the two SAR images (e.g. Zebker et al., 2000; Simons and Rosen, 2015). The degree of coherence loss (decorrelation) further varies regionally and seasonally with topography and atmospheric water vapor. Atmospheric water vapor can significantly alter the propagation of radar waves and impose apparent ground motion, though longer wavelengths are less affected (e.g. Foster et al., 2006; Ding et al., 2008; Sandwell et al., 2008; Wei and Sandwell, 2010; Malinverni et al., 2014; Parker et al., 2015).

2.2.2 Formation of SAR volcano deformation database

We compile global observations of volcano deformation from: Biggs and Pritchard (2017), the Smithsonian Institution's Global Volcanism Program Volcanoes of the World database, and the Centre for Observation and Modelling of Earthquakes, Volcanoes and Tectonics (COMET) Global Volcano Deformation Database. Our final database has been synchronized with Biggs and Pritchard (2017), Ebmeier et al. (2018), and Biggs et al. (2014),

though ours excludes volcanoes with only ground-based measurements or events with a suspected non-magmatic cause (with inferred source causes listed by the author(s) of the published deformation event that were obviously non-magmatic such as ‘lava subsidence’ or ‘anthropogenic’). For the purpose of assessing the utility of the satellite methodology, we used observations of deforming volcanoes measured by SAR satellites though not necessarily measured exclusively by SAR satellites (i.e. deformation may also have been measured by GPS, for example). We further only report episodes of deformation included in peer-reviewed publications. Our spatial database contains 147 volcanoes with deformation using data from approximately a dozen satellites (in supplementary Table 1). The timing deformation database only includes volcanoes that had eruptions between 1978-2016, which includes 71 volcanoes (see supplementary Table 2).

2.3 UV spectroscopy database

2.3.1 UV data

Using satellites to measure volcanic SO₂ emissions was not considered until the eruption of El Chichòn volcano, Mexico, in 1982, when its eruption plume dominated the measurement by the Total Ozone Mapping Spectrometer (TOMS) instrument on the Nimbus-7 satellite (Krueger, 1983). As TOMS was not initially intended for measurement of volcanic SO₂, large degassing events – primarily eruptions – were needed to substantially affect the ozone retrievals and provide a measurement of column SO₂ amounts (e.g. Carn et al., 2003). The TOMS records were therefore used principally to quantify volcanic SO₂ emissions during eruptions and not to detect precursory eruptive emissions.

Even though H₂O and CO₂ are the most abundant volcanic gases, their large atmospheric background levels render them difficult to detect via satellite (e.g. Carn et al., 2016; although

satellite capabilities to detect CO₂ are emerging, see Schwandner et al., 2017). In contrast, SO₂ has low background concentrations and high concentrations in volcanic clouds, so it has been the focus of satellite remote-sensing degassing studies (e.g. Krueger et al., 2000; Carn et al., 2003). Additionally, while volcanic ash is an important component of volcanic gas spectroscopy and thermal remote-sensing, we do not include these measurements in our database. Ash clouds are only generated during the eruptive phase, and our research focuses on volcanic activity which may forewarn of an eruption.

In 2004, the Ozone Monitoring Instrument (OMI) was launched aboard the NASA Aura satellite with the specific purpose of assessing daily vertical column SO₂, ozone, and other trace gases (e.g. Carn et al., 2013). With increased sensitivity, OMI allows measurement of smaller, eruptive degassing as well as more persistent and passive degassing from both volcanic and anthropogenic sources (e.g. McCormick et al., 2012; Fioletov et al., 2016; Carn et al., 2017).

Ultraviolet sensors only operate by day and their detection limits vary as a function of altitude, latitude, and season (see Table 1 for instrument specifications for TOMS and OMI sensors, including lifespans, resolutions, and detection thresholds). It is easier to detect SO₂ at higher altitudes because this minimizes atmospheric path length, and thus opportunities for scattering and absorption of solar photons by other atmospheric gases (e.g. McCormick et al., 2013). Regions closer to the poles also have higher detection limits because they exhibit reduced UV during winter, higher ozone levels, are close to the boundary between the day and night terminator (line separating sun coverage of day from night); conversely, tropical latitudes are more often plagued by cloud coverage (e.g. Carn et al., 2003). Reduced sunlight means winter months are also particularly challenging (e.g. McCormick et al., 2013). These conditions

complicate measurement of emissions in certain regions like Alaska, Kamchatka, and the Kurile Islands (e.g. Carn et al., 2013), which collectively host hundreds of active volcanoes.

2.3.2 Formation of UV/VIS volcano SO₂ emissions database

We use the Multi-Satellite Volcanic Sulfur Dioxide L4 Long-Term Global Database V2 (Carn, 2015) with measurements of SO₂ emissions dominated by volcanic eruptions between 1978 to 2016. We also incorporate the names of volcanoes with passive SO₂ emissions listed in Carn et al. 2017, however the passive emissions do not contain time of measurement so we do not use them to compare timing between emission and eruption in section 3.3. The “eruptive SO₂ emissions” and “passive SO₂ emissions” databases are mostly composed of detection by TOMS and OMI sensors, though other sensors operating in the ultraviolet to infrared range have been used in satellite studies of volcanic degassing (e.g. Realmuto et al., 1997; Corradini et al., 2010; Theys et al., 2013), and some of these (e.g. Ozone Mapping Profiler Suite, Atmospheric Infrared Sounder, Infrared Atmospheric Sounding Interferometer) were used to supplement the database (Carn et al., 2017). Our global compilation of volcanic SO₂ degassing measured by satellite includes 173 volcanoes with measurable emissions (spatial database with both eruptive and passive emissions, see supplementary Table 5) and the timing database includes 118 volcanoes (mostly eruptive emissions, see supplementary Table 6).

2.4 Recently erupting volcanoes database

We used the historical database of eruptions from the Global Volcanism Program (2013), wherein an eruption is defined by events that involve the explosive ejection of fragmental material, effusion of molten lava, or both (Siebert et al., 2010). From this we extracted a global list of eruptions between 1978 and 2016. The eruption start and end dates reported by the Global

Volcanism Program (2013) contain uncertainties (quantified in the database where applicable) as well as recording biases though this is an issue intrinsic to any historical database. Their database includes start dates with year, month when known (53% of eruptions on file), and day when known (41% of eruptions on file), while the end dates are only reported for 59% of the eruptions on file. See “Volcanoes of the World, Third Edition” by Siebert et al. (2010) for more details.

We downloaded eruptions with either start or end dates of 1978 or later from the Global Volcanism Program (2013) and removed eruptions from all submarine volcanoes, except for three, where satellite imagery is generally not useful. The three submarine volcanoes that produced satellite-detections are: Kavachi volcano (Solomon Islands, with satellite-detections by MODVOLC: Wright et al., 2014); Hunga Tonga-Hunga Ha’apai volcano (Tonga, with satellite-measured SO₂: Carn. 2015) and Home Reef volcano (Tonga, with measured SO₂ emissions: Carn, 2015). To include the full satellite lifespan we choose 1978 as the start date for this study: the beginning of global coverage for UV devices was 1978, for SAR devices was 1992, and for TIR devices was 2000. This recent eruptions list includes 250 unique volcanoes (spatial eruptions database, in supplementary Table 7). The eruptions database used to compare timing between satellite-detected activity and eruptions additionally includes the last prior known eruption to 1978 as well as eruptions between 1978-2016 (timing eruptions database, in supplementary Table 8).

2.5 Timing between satellite-detected activities and recent eruptions

We explore the temporal relationship between eruption and satellite-detections from each SAR, UV (mostly eruptive emissions), and TIR (only MODVOLC data due to its high temporal resolution) sensors. We used our list of volcanoes with satellite-detections that had recently erupted and compared periods of eruptions (start and end dates from Global Volcanism Program,

(2013), supplementary Table 8) to start dates of reported satellite-detections (supplementary Tables 2, 4, and 6), comparing each satellite-detections database to eruptions separately.

It should be stated that there are multiples challenges with calculating timing between satellite-measured activities and eruptions. First and foremost, the start and especially the end date for an eruption can be uncertain (e.g. Siebert et al., 2010). This is especially a problem for persistently active volcanoes where eruptions wax and wane, and it is not clear how to define when one eruption ends and another begins. This implies that any satellite-detected activity at persistently active volcanoes could just as easily be considered pre-eruptive, co-eruptive, or post-eruptive. Similarly, the defined start and end dates for satellite-detected activities are prone to aforementioned issues with sensor detection threshold and non-continuous satellite coverage which make it challenging to parse separate satellite-detected activities. In certain situations, satellite coverage begins after an eruption has already commenced, or only in hindsight is a satellite-detected activity considered pre-eruptive or non-eruptive. These issues are intrinsic to an analysis of timing between satellite-detected activities and eruptions, and, as such, there are multiple ways to analyze the data depending upon the chosen definitions.

The start date of each satellite-detected activity is compared to the eruption start and end dates to find the closest eruption in time. If a volcano where we have a satellite-detected activity has no eruptive record or no eruption within 30 years either prior to or after the satellite-detection, the satellite-detection is deemed non-eruptive. If there is an eruption within 30 years of the satellite-detection, we associate the satellite-detection with the eruption in one of three ways: pre-eruptive, co-eruptive, and post-eruptive satellite-detected activities. Our definition for the pre-eruptive interval lasts from the midpoint between the end of the prior eruption and the start of the next, the post-eruptive interval lasts from the end of an eruption to the midpoint between

the end of that eruption and the next, and the co-eruptive interval defines the timing between the start of an eruption and its end (see Figure 1). By these definitions, a post-eruptive activity may later be considered pre-eruptive, though this would only affect the most recent eruptions at a volcano.

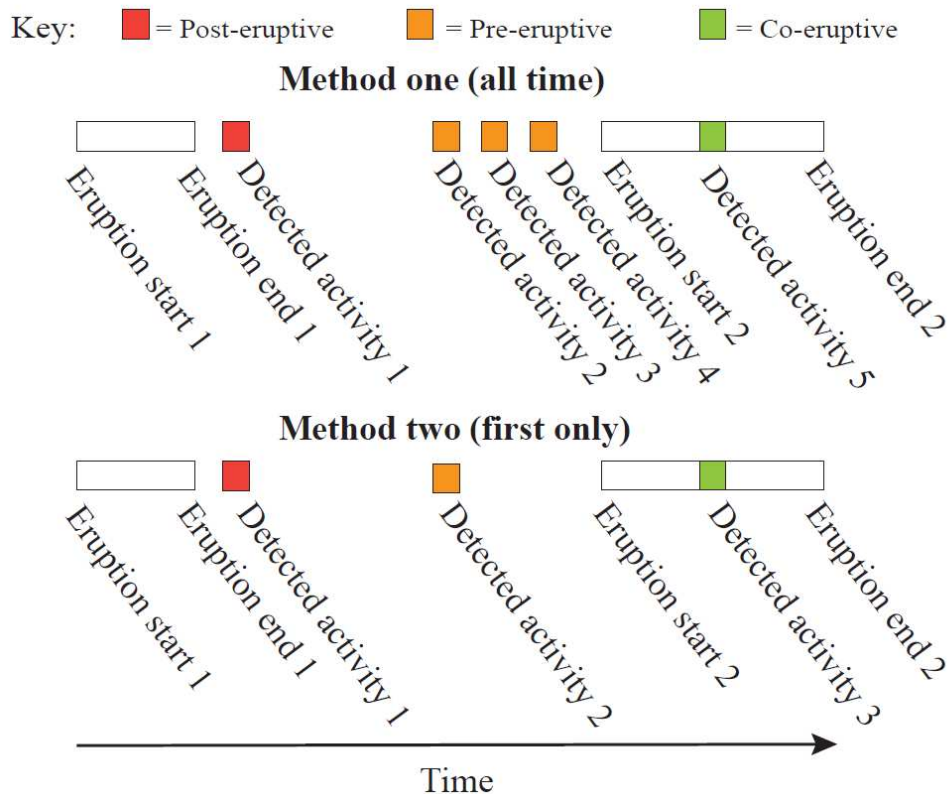


Figure 1. Conceptual diagram to illustrate the two types of methods used to compare timing between satellite-detections and eruptions. Boxes represent individual detections and their widths correspond with their duration. The top image compares timing between all satellite-detections and eruptions whereas the latter uses only the first detection if there are multiple. Colors denote the classification of the detected activity in terms of the three categories: post-, pre-, and co-eruptive activities. This analysis is performed separately for each type of satellite-detection (deformation, SO₂ degassing, thermal).

We choose two different methods to analyze the data, but other methods may be equally justified. Method one incorporates all satellite-detected activities while method two uses only the first satellite-detected activity in a pre-eruptive period, in the case where there are multiple

satellite-detected activities that occur before an eruption (refer to Figure 1). Method one includes multiple pre-eruptive satellite-detections for each eruption, while method two does not. Negative values were assigned for satellite-detections occurring before eruption start dates (pre-eruptive), zero values were assigned for satellite-detections occurring between the eruption start and end dates (co-eruptive), and positive values were assigned for satellite-detections occurring after eruption end dates (post-eruptive).

3 Results and Analysis

3.1 Comparing volcanoes with satellite-measured activities to eruptions

Comparing these three compilations of volcanoes with satellite-detected activities from SAR sensors, TIR sensors, and UV spectroscopy sensors described in the previous sections produces a database of 306 unique volcanoes with at least one type of satellite-detection (Figure 2, and supplemental Tables 1, 3, and 5). Of the 306 unique volcanoes with satellite-detections in our database, 196 have experienced recent eruption. Seventy-eight percent of volcanoes that have erupted since 1978 (196/250) are also associated with detection by at least one type of satellite sensor. Of those volcanoes with detection by just one type of sensor (Figures 2a and 2b), 44% recently erupted [84 erupting volcanoes with one type of satellite-detection/(106 non-erupting volcanoes with one type of satellite-detection + 84 erupting volcanoes with one type of satellite-detection)]. For those volcanoes with detection by two types of satellite sensors (Figures 2c and 2d), 96% recently erupted [69 erupting volcanoes with detection by two types of satellite sensors/(69 erupting volcanoes with detection by two types of satellite sensors + 3 non-erupting volcanoes with detection by two types of satellite sensors)]. Lastly, of those volcanoes with detection by three types of satellite sensors (Figures 2e and 2f), 98% recently erupted [43 erupting volcanoes with detection by three types of satellite sensors/(43 erupting

volcanoes with detection by three types of satellite sensors + 1 non-erupting volcano with detection by three types of satellite sensors)]. Lastarria (Chile) is the only non-erupting volcano with detection by three types of satellite sensors (Figure 2e).

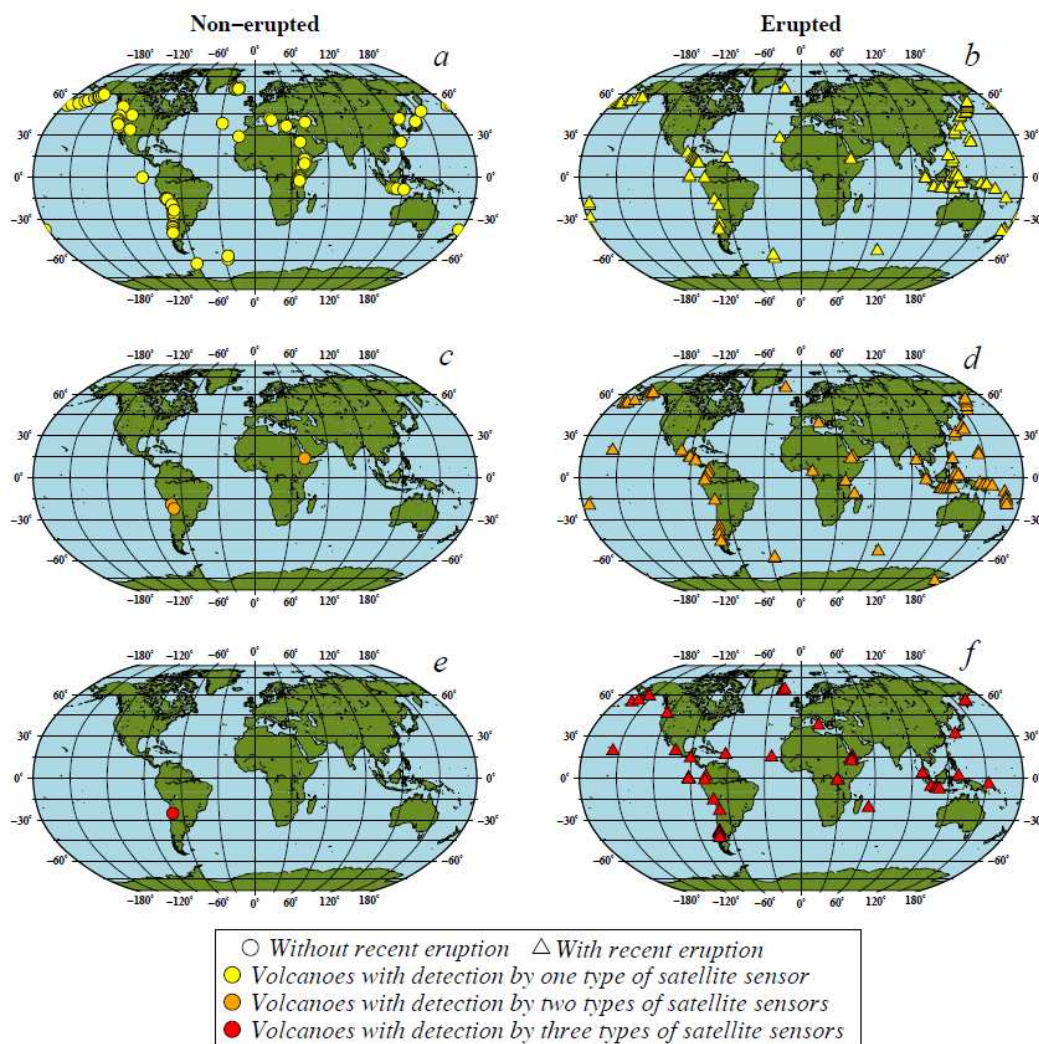


Figure 2. 306 subaerial volcanoes with detection by at least one type of satellite sensor (deformation, thermal, SO₂ degassing, in supplemental material Tables 1, 3, and 5) between 1978 and 2016. 196 of these volcanoes have also erupted during this time period. As we do not include all possible satellites, there are likely more satellite measurements than are displayed here. The figures on the left include volcanoes with detection by at least one type of satellite sensor that did not erupt between 1978 and 2016. The figures on the right include volcanoes with detection by at least one type of satellite sensor that erupted between 1978 and 2016.

The distribution of volcanic satellite-detected activities through time is shown in Figure 3. Fewer than 100 activities were detected by satellite every year between 1978 and 2000, after which 100s to 1000s of activities were detected by satellite every year. This jump in the year 2000 coincides with the launch of the thermal infrared sensor, MODIS. The number of satellite-detections per year is also compared to the number of erupting volcanoes per year in Figure 4. From 1978-2016 there were roughly 20-45 subaerial eruptions per year. During this time, satellites detected eruptions at 1-25 volcanoes per year and did not detect eruptions at 1-10 volcanoes per year.

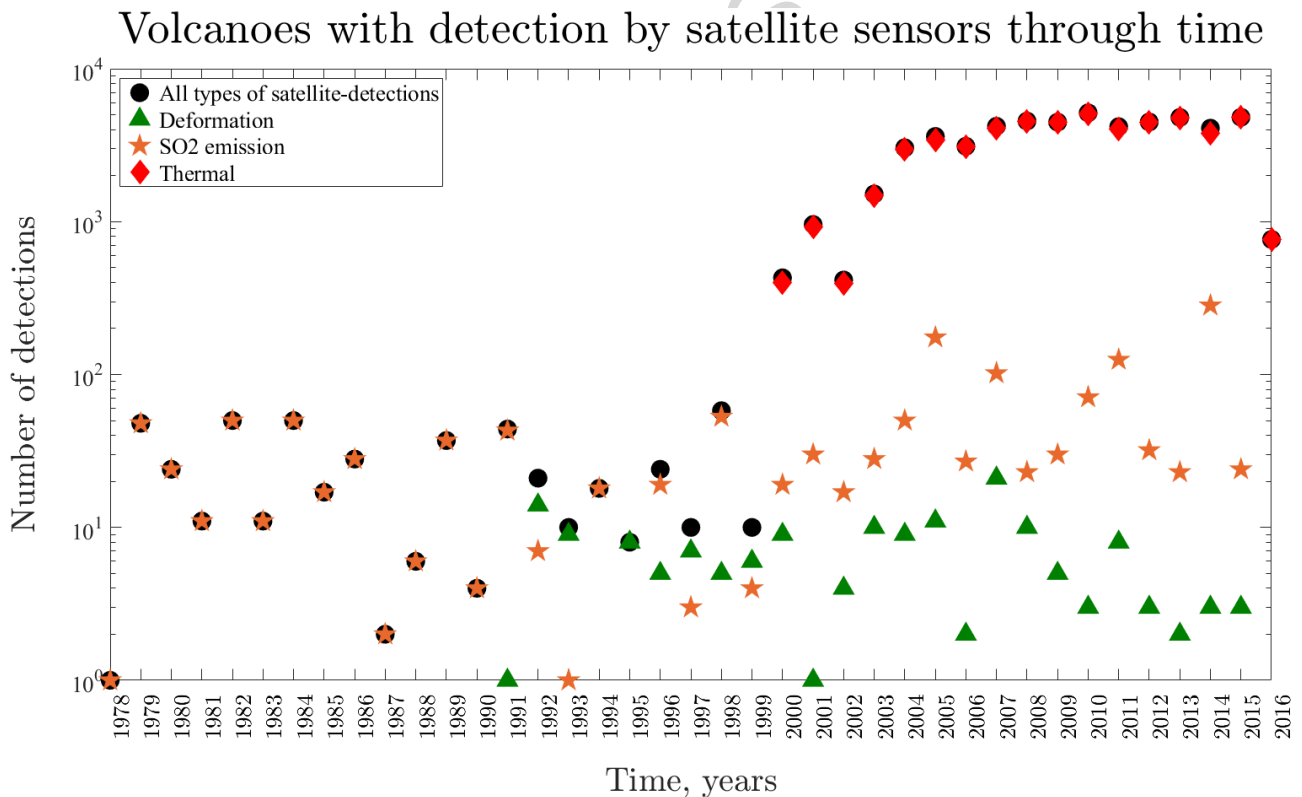


Figure 3. Number of volcanoes with detection by at least one satellite sensor per year between 1978 and 2016. Total number of volcanoes with detection by satellite sensors is shown as black circles, whereas the other colors and symbols denote the type of sensor. (See legend). Volcanic activity is binned into yearly data according to the start of the satellite-detected activity. We suspect the decrease in the number of satellite detections in 2016 is related to data processing and publication lags and these values should increase in the near future. (We only include published reports of deformation, the latest deformation data are available online: volcanodeformation.blogs.ilrt.org).

Erupting volcanoes through time as measured/not measured by satellite

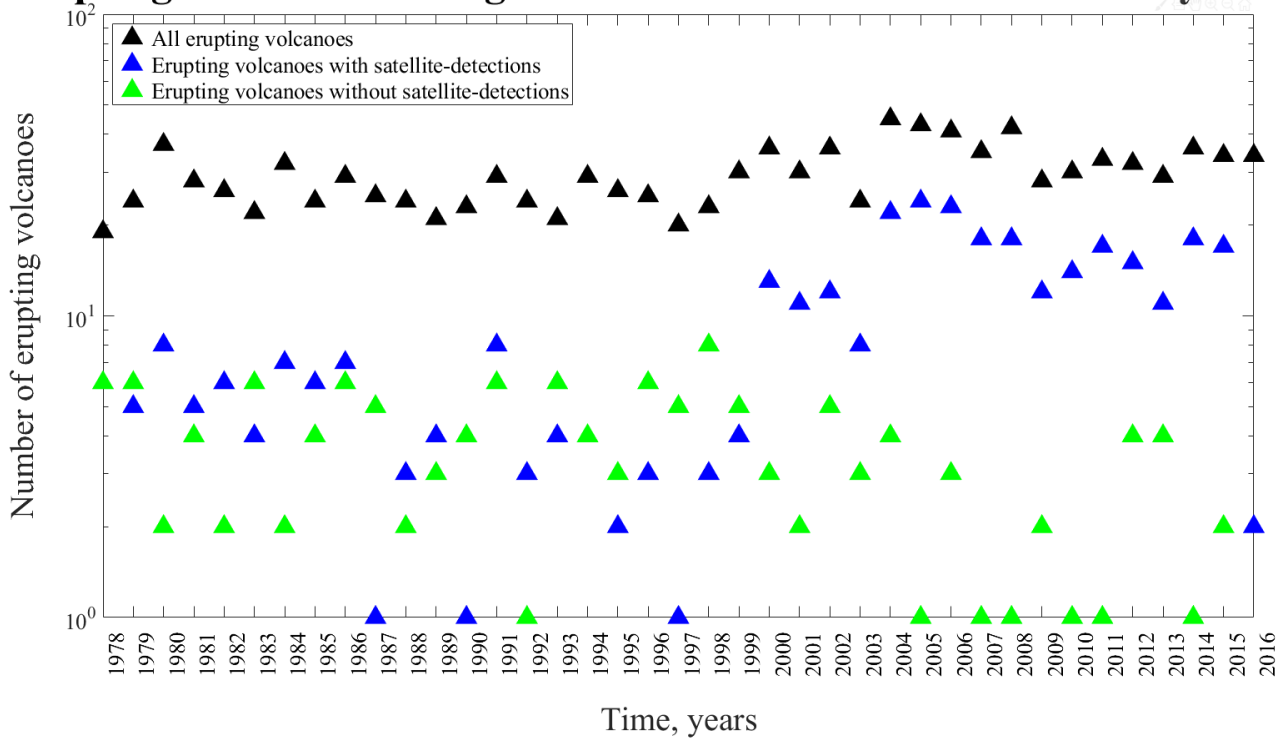


Figure 4. Number of volcanoes erupting through time during the satellite era (1978-2016, eruption data from the Global Volcanism Program, (2013)). Eruptions are binned into yearly data according to the start date of the eruption. Black indicates all subaerial volcanic eruptions between 1978 and 2016 (no size threshold), while blue indicates volcanoes with satellite-detections that also erupted. Volcanoes with satellite-detections and eruption are binned into yearly data based on the start date of the satellite-detection. The decrease in the number of satellite-detections in 2016 is likely related to data processing and publication lags for deformation data (we only include published reports) and these values should increase in the near future.

Our null hypothesis is that the eruption rate of volcanoes with satellite-detections is the same as the eruption rate of volcanoes without detection by satellite sensors. Figure 5 provides a contingency table for testing the statistical significance of volcanoes with satellite-detections to volcanoes that had eruptions between 1978 and 2016 (e.g. Biggs et al., 2014; Begeuría, 2006).

The statistical terms used are referred to as the positive and negative predictive values, though in this case “predictive” refers to the statistical link between attributes and does not imply that the

All satellite-detected activities

	Erupted, E	Non-erupted, \bar{E}	<i>a</i>
Satellite-detection, \bar{U}	True positive 196	False positive 110	Satellite-detections row total 306
Absence of a satellite-detection, U	False negative 54	True negative 1055	Absence of a satellite-detection row total 1109
	Erupted column total 250	Non-erupted column total 1165	Total number subaerial volcanoes 1415

Satellite-detected deformation

	Erupted, E	Non-erupted, \bar{E}	<i>b</i>
Satellite-detected deformation, \bar{U}	True positive 71	False positive 76	Satellite-detected deformation row total 147
Absence of satellite-detected deformation, U	False negative 179	True negative 1089	Absence of satellite-detected deformation row total 1268
	Erupted column total 250	Non-erupted column total 1165	Total number subaerial volcanoes 1415

Satellite-detected thermal anomalies

	Erupted, E	Non-erupted, \bar{E}	<i>c</i>
Satellite-detected thermal feature, \bar{U}	True positive 112	False positive 34	Satellite-detected thermal feature row total 146
Absence of satellite-detected thermal feature, U	False negative 138	True negative 1131	Absence of satellite-detected thermal feature row total 1269
	Erupted column total 250	Non-erupted column total 1165	Total number subaerial volcanoes 1415

Satellite-detected SO₂ degassing

	Erupted, E	Non-erupted, \bar{E}	<i>d</i>
Satellite-detected SO ₂ degassing, \bar{U}	True positive 168	False positive 5	Satellite-detected SO ₂ degassing row total 173
Absence of satellite-detected SO ₂ degassing, U	False negative 82	True negative 1160	Absence of satellite-detected SO ₂ degassing row total 1242
	Erupted column total 250	Non-erupted column total 1165	Total number subaerial volcanoes 1415

Figure 5. Contingency table to compare volcanoes with satellite-detection and those with eruptions between 1978-2016, no-size threshold (see Figures 2, and supplemental Tables 1, 3, 5, and 7) from the Global Volcanism Program (2013). The meaning of these values is provided in detail in the main text.

satellite-detected activity precedes an eruption. For all types of satellite-detected activities (Figure 5a) we determine the positive predictive value to be 0.64 [true positives/(true positives + false positives)], which demonstrates the proportion of volcanoes with satellite-detections that were associated with volcanoes that recently erupted. The negative predictive value [true negatives/(true negatives + false negatives)] is 0.95, indicating the proportion of volcanoes without satellite-detections that also did not erupt since 1978.

The sensitivity of our analysis [true positives/(true positives + false negatives)] is 0.78 and the specificity [true negatives/(false positives + true negatives)] is 0.91. The sensitivity describes the proportion of positive cases (satellite-detections and eruption) correctly predicted whereas the specificity describes the proportion of negative cases (no satellite-detections, no eruption) correctly predicted. The standard eruption rate, represented by the positive predictive value of volcanoes that also recently erupted (250 with recent eruption/1415 subaerial Holocene volcanoes), is 0.18. We reject our null hypothesis given that the standard eruption rate is much lower than our satellite-detected eruption rate. Thus, the eruption rate of volcanoes with satellite-detections is clearly higher than the eruption rate of volcanoes without satellite-detection.

We also test the statistical significance in contingency tables between volcanoes with eruptions and volcanoes with satellite-detections by the individual sensors: SAR, TIR, and UV (Figures 5b, 5c, and 5d). The positive predictive values [true positives/(true positives + false positives)] for each SAR, TIR, and UV, respectively, are: 0.48, 0.77, 0.97 while the negative predictive values [true negatives/(true negatives + false negatives)] are 0.86, 0.89, 0.94. The sensitivity [true positives/(true positives + false negatives)] of each is: 0.28, 0.45, 0.67, and the specificity [true negatives/(false positives + true negatives)] of each is: 0.94, 0.97, 1. Biggs et al. (2014) performed a similar analysis using 198 volcanoes with systematic observations of

deformation (also satellite-based) over 18 years. Their findings are similar to ours: a positive predictive value of 0.46 and a negative predictive value of 0.94 (Biggs et al., 2014).

3.2 Eruptions without satellite-measured activity

Since 1978, 54 volcanoes have had recent eruptions (135 eruptions) without detection by the satellite sensors considered in our database (Figure 6). The majority of these eruptions were small (Figure 7), with volcanic explosivity index (VEI) between 0 and 3 (Global Volcanism Program, 2013), though VEI 2 is the default value for effusive eruptions. Only four eruptions (4/135) were VEI 3 and had no satellite detections (in supplementary Table 11). These lower-VEI eruptions are less energetic and may not project as high in the atmosphere as the higher-VEI eruptions, and any pre-eruptive degassing would similarly reflect low-magnitude emissions (Carn et al., 2016). At least 87% of lower VEI eruptions (≤ 2) either do not degas or do not degas sufficiently to be measured by satellite sensors, though this may somewhat reflect eruptions that have not yet been investigated in detail (Carn et al., 2016). Given the large quantity of satellite data and frequent eruptions of small VEI, not all emissions have been analyzed (Carn et al., 2016). The TOMS sensors specifically did not measure low VEI eruptions ($\text{VEI} < 4$) unless they were particularly sulfur-rich (e.g. Carn et al., 2009a). This meant that lower-VEI eruptions and emissions were much less likely to be detected by UV satellite sensors that have higher detection limits at lower altitudes, although the increased sensitivity of OMI can measure passive degassing at volcanoes not previously detectable with TOMS (e.g. Carn et al., 2017).

Looking at the Bulletin Reports of the Global Volcanism Program (2013) for each of these 54 volcanoes (in detail in supplementary Table 11), 12 (12/54) of these volcanoes had eruptions preceded only by notable changes to seismicity while 26 (26/54) of these volcanoes had eruptions that were not preceded by any type of detection, even from ground-based sensors.

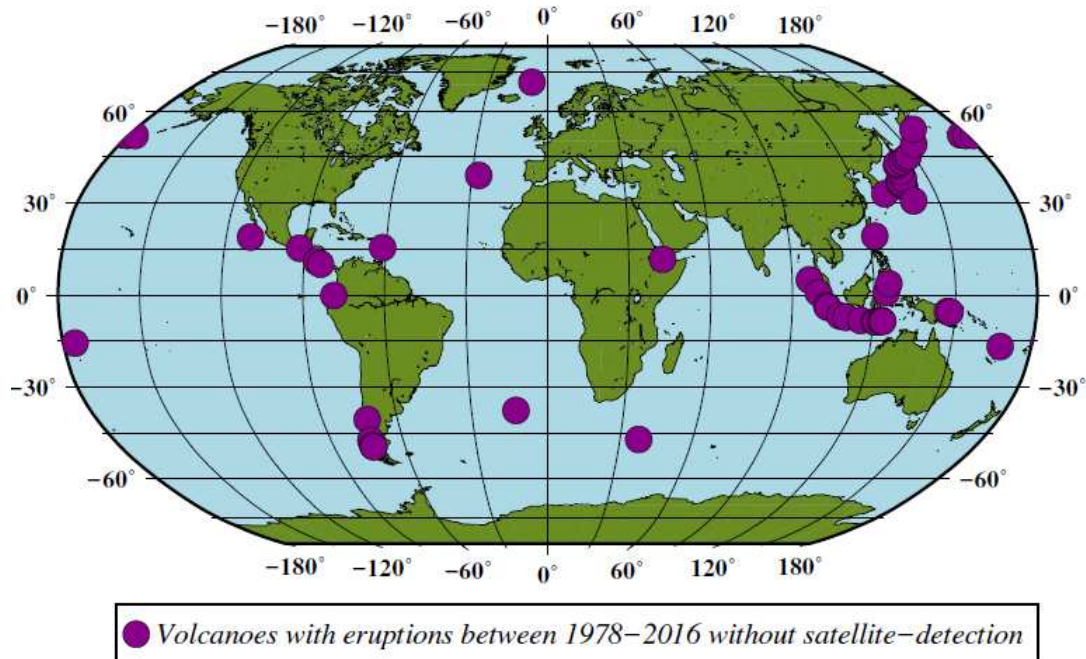


Figure 6. 54 volcanoes with eruptions in the satellite era (defined here as 1978-2016, from Global Volcanism Program (2013)) without satellite-detections from the three satellite methods considered here.

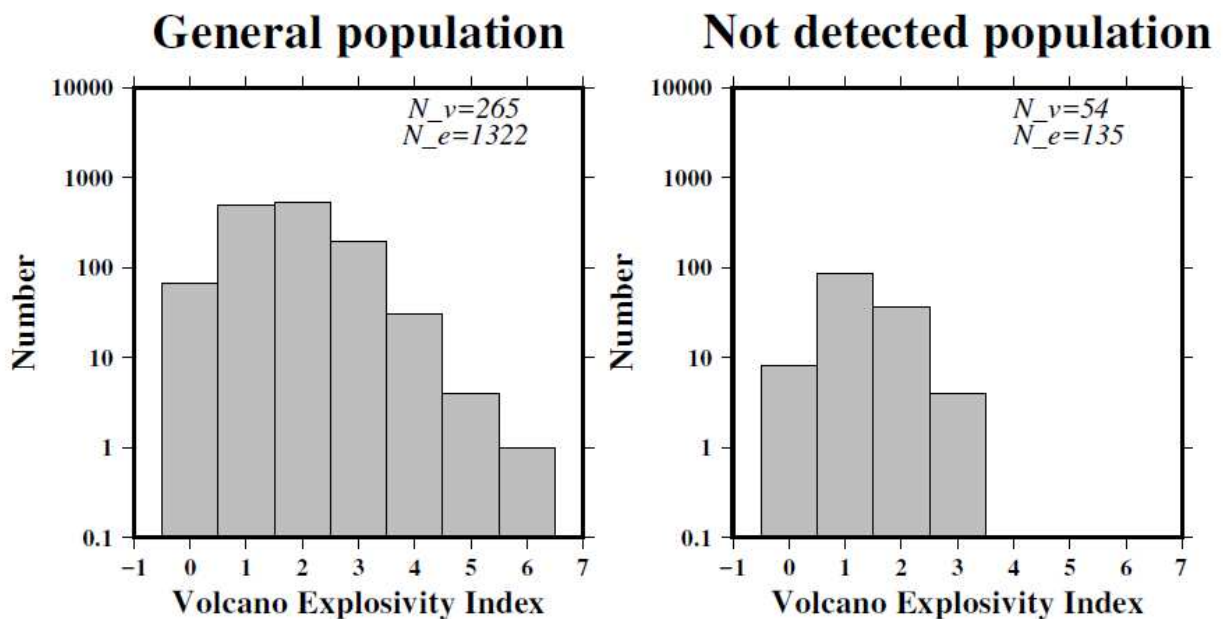


Figure 7. Left: Volcanic explosivity indexes (Global Volcanism Program, 2013) of confirmed eruptions for all subaerial volcanoes that erupted between 1978 and 2016. Right: Volcanic explosivity indexes (Global Volcanism Program, 2013) of confirmed eruptions for each of the 54 volcanoes without satellite-detections. The shorthand “N_e” stands for number of episodes while “N_v” stands for number of volcanoes.

The other 16 volcanoes (16/54) produced ground-detections prior to their eruptions, though many of these eruptions occurred in the early days of satellite remote sensing when detection thresholds were high. For the more recent eruptions, we speculate that the satellite overpass did not occur at the opportune time or the detection thresholds of the sensors were still too high. As listed in more detail in the supplemental material (supplementary Table 11), a handful of these volcanoes have co-eruptive satellite-detections from other sensors that are listed in the Global Volcanism Program but were not included in our catalogues (e.g. the Advanced Very High Resolution Radiometer thermal sensor). Additionally, Hakoneyama volcano, and perhaps others, were detected by InSAR but these results were not published in peer-reviewed journals and so were not included in our database.

To further investigate the eruptions with ground-based detections that were not found by satellite, we review the higher-spatial resolution ASTER data for some of these volcanoes. In the interest of time, we reviewed ASTER scenes for 35 volcanoes that erupted between 1978-2016 without satellite-detections. We reviewed all scenes between 2000-2016 (where cloud coverage was less than 25% of the image) and note that at least 14 of these volcanoes contain likely thermal features that merit further study (see supplementary Figures 1-11 and supplementary Table 10). We also note that while ASTER data do exist for each of these volcanoes, in some cases the data can be too sparse to define timing between thermal features and eruption.

3.3 Timing between satellite detections and eruption

We used two methods to define time intervals between satellite-detections and eruptions, described in section 2.6. The first method includes all satellite-detections and the second method includes only the first satellite-detection. The data are also divided into three eruptive intervals: pre-eruptive, co-eruptive, and post-eruptive. These data are displayed in Figure 8.

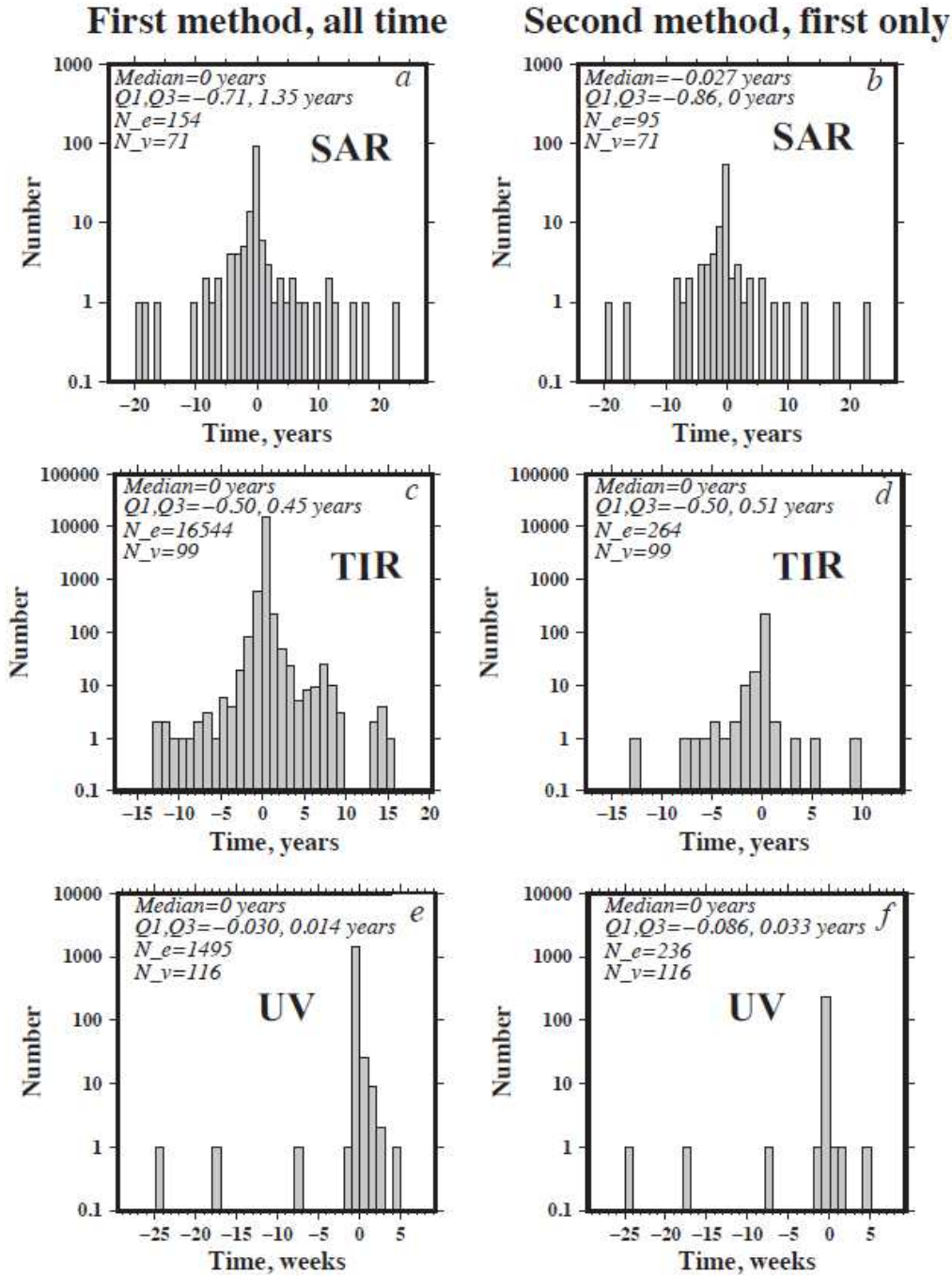


Figure 8. Time between satellite-detected activities from each sensor and eruption (Global Volcanism Program, 2013). The left column shows all detections (method one) while the right column shows only the first in sequence (method two). Figures 8a and 8b show satellite-detected deformation from SAR sensors, Figures 8c and 8d show satellite-detected thermal features from TIR sensors, and Figures 8e and 8f show satellite-detected SO₂ degassing from UV sensors. The shorthand “N_e” stands for number of episodes, “N_v” stands for number of volcanoes, and “Q1” and “Q3” refer to the first and third quartile, respectively.

The median time interval between deformation episodes and eruption start dates according to the first method (all time, see Figure 8a) is zero years before an eruption (first quartile is 0.71 years before an eruption and third quartile is 1.35 years after an eruption) as compared to 0.03 years before an eruption by the second method (first quartile is 0.86 years before an eruption, third quartile is zero years, see Figure 8b). However, in both cases, most of the detections occur during the pre-eruptive period (49% and 57%, respectively, see Table 2). The SAR data used here do not represent continuous coverage of each volcano, and some of the data are aliased due to satellite overpass frequency. The defined start and end dates probably do not often coincide with the actual duration of the deformation episode, but rather correspond with durations of observation. As the upper bound on satellite repeat intervals using SAR data recur approximately monthly, the reported timings between deformation start dates and eruption start dates are not exact and should only be regarded as accurate to within a few months. We are unable to formalize the errors given that continuous coverage does not yet exist.

The median timing between satellite detections from TIR sensors and eruption is zero years by the first method (first quartile is 0.5 years before an eruption, third quartile 0.45 years after an eruption, see Figure 8c) and zero years by the second method (first quartile 0.5 years before an eruption, third quartile 0.51 years after an eruption, see Figure 8d). For both methods most of the detections occur during the co-eruptive period (88% and 76%, respectively, see Table 2), and this is not surprising since this dataset is entirely MODVOLC, and that mostly captures eruptive episodes.

For SO₂ emissions, the first method finds a median time of zero years (first quartile is 0.03 years before an eruption, third quartile is 0.01 years after an eruption) and the second method a median time of zero years (first quartile is 0.09 years before an eruption, third quartile

is 0.03 years after an eruption, see Figures 8e and 8f). For each method, the majority of the SO₂ emissions occur within the co-eruptive period (97% and 96%, respectively, see Table 2) and this is to be expected given that the SO₂ compilation includes mostly co-eruptive measurements.

One issue with both of our methods of comparing satellite-detections to eruptions is that pre-eruptive and post-eruptive values cancel each other, so we also isolate the pre-eruptive and post-eruptive intervals for the first method and report median values for each (Figure 9).

Isolating the pre-eruptive period suggests the chronology of a satellite-detection before an eruption (assuming current and past detection thresholds and analysis in real-time). When we limit our data to only pre-eruptive satellite-detections (Figure 9a, 9c, 9e), deformation (N=75) occurred a median of 0.71 years before an eruption (first quartile 2.2 years before an eruption, third quartile 0.08 years after an eruption), thermal features (N=947) occurred a median of 0.5 years before an eruption (first quartile 0.9 years before an eruption, third quartile 0.2 years after an eruption), and SO₂ degassing (N=7) occurred a median of 0.03 years before an eruption (first quartile 0.3 years before an eruption, third quartile 0.003 years after an eruption).

4 Discussion

4.1 Timing between satellite-detections and eruption

Our first method of analysis between satellite-detections and eruptions through all time contextualizes satellite detections in the eruption cycle. This analysis suggests that deformation episodes are largely pre-eruptive. In contrast, thermal features are largely co-eruptive, yet our analysis solely uses data from MODVOLC. We discussed previously that dependence on a low-resolution TIR sensor can fail to detect thermal features which may occur prior to (or even during) an eruption, although the lower-spatial resolution SEVIRI sensor (ground resolution of 3 km, repeat interval of 15 minutes) has demonstrated the ability to detect precursory

Description	Deformation (our study, method one)	Deformation (our study, method two)	Deformation (<i>Biggs et al., 2014</i>)	Thermal (our study, method one)	Thermal (our study, method two)	SO ₂ (our study, method one)	SO ₂ (our study, method two)
# episodes	153	94	40	16475	261	1494	235
# volcanoes	71	70	29	98	97	116	116
# pre-eruptive	75	54	n/a	947	49	7	6
# co-eruptive	44	19	n/a	14368	199	1449	226
# post-eruptive	34	21	n/a	1160	13	38	3
% pre-eruptive	49%	57%	51%	5%	19%	0%	3%
% co-eruptive	29%	20%	13%	88%	76%	97%	96%
% post-eruptive	22%	23%	36%	7%	5%	3%	1%
Median	0 (days)	-11 (days)	n/a	0 (days)	0 (days)	0 (days)	0 (days)
First quartile	-241 (days)	-313 (days)	n/a	0 (days)	0 (days)	0 (days)	0 (days)
Third quartile	0 (days)	0 (days)	n/a	0 (days)	0 (days)	0 (days)	0 (days)
Min value	-7027 (days)	-7027 (days)	n/a	-4625 (days)	-4625 (days)	-171 (days)	-171 (days)
Max value	8219 (days)	8219 (days)	n/a	5590 (days)	3307 (days)	30 (days)	30 (days)

Table 2. Timing between detections and eruption through the pre-, co-, and post-eruptive periods (data are displayed in Figure 8). “Pre-eruptive”, “co-eruptive”, and “post-eruptive” values should be considered together (add up to 100%).

USCRIPT

activity before MODVOLC (e.g. Mount Etna (Italy) in 2008: Ganci et al., 2011). A higher-resolution TIR sensor may also provide more warning, and indeed some studies have demonstrated that the higher spatial resolution ASTER sensor can detect thermal features a few months prior to an eruption (e.g. Pieri and Abrams, 2005; Delgado et al., 2014; Reath et al., 2016). Like the thermal results, SO₂ emissions occur mostly during the co-eruptive period which is to be expected given the eruptive bias in our database. The first few decades of volcanic SO₂ measurements (1978-2004) are dominated by the TOMS sensors which were not initially intended for use in measuring volcanic gas emissions. Measurement of passive emissions (or non-obvious eruptive emissions) requires more sensitivity and has been monitored better using OMI as well as infrared sensors such as ASTER and MODIS (e.g. Realmuto, 1999; Campion, 2010; Thomas and Watson, 2010). Indeed, many scientists have emphasized the importance of passive emissions, arguing these may be responsible for the majority of volcanic SO₂ output (e.g. Berresheim and Jaeschke, 1983; Carn et al., 2003; Carn et al., 2008; Bani et al., 2012; McCormick et al., 2012; Carn et al., 2017). Recent research has also demonstrated that slightly increased, passive SO₂ emissions were measurable in the few years before an eruption utilizing OMI and specialized data processing methods (e.g. Carn et al., 2017 reported: Aso (Japan) had increased emissions measured in 2011 prior to the 2014 eruption; SO₂ was measured from Sarychev Peak (Kuril Island) in 2005 prior to the 2009 eruption; and SO₂ was measured at Aludafilla (Ethiopia) in 2005 prior to the 2008 eruption).

By isolating the pre and post-eruptive periods we find a median timing between eruptions and satellite-detections of: -0.7 years (pre-eruptive SAR), -0.5 years (pre-eruptive TIR), -0.03 years (pre-eruptive UV), and 1.4 years (post-eruptive SAR), 0.5 years (post-eruptive TIR), and 0.01 years (post-eruptive UV). The lengthy pre- and post-eruptive measurements we

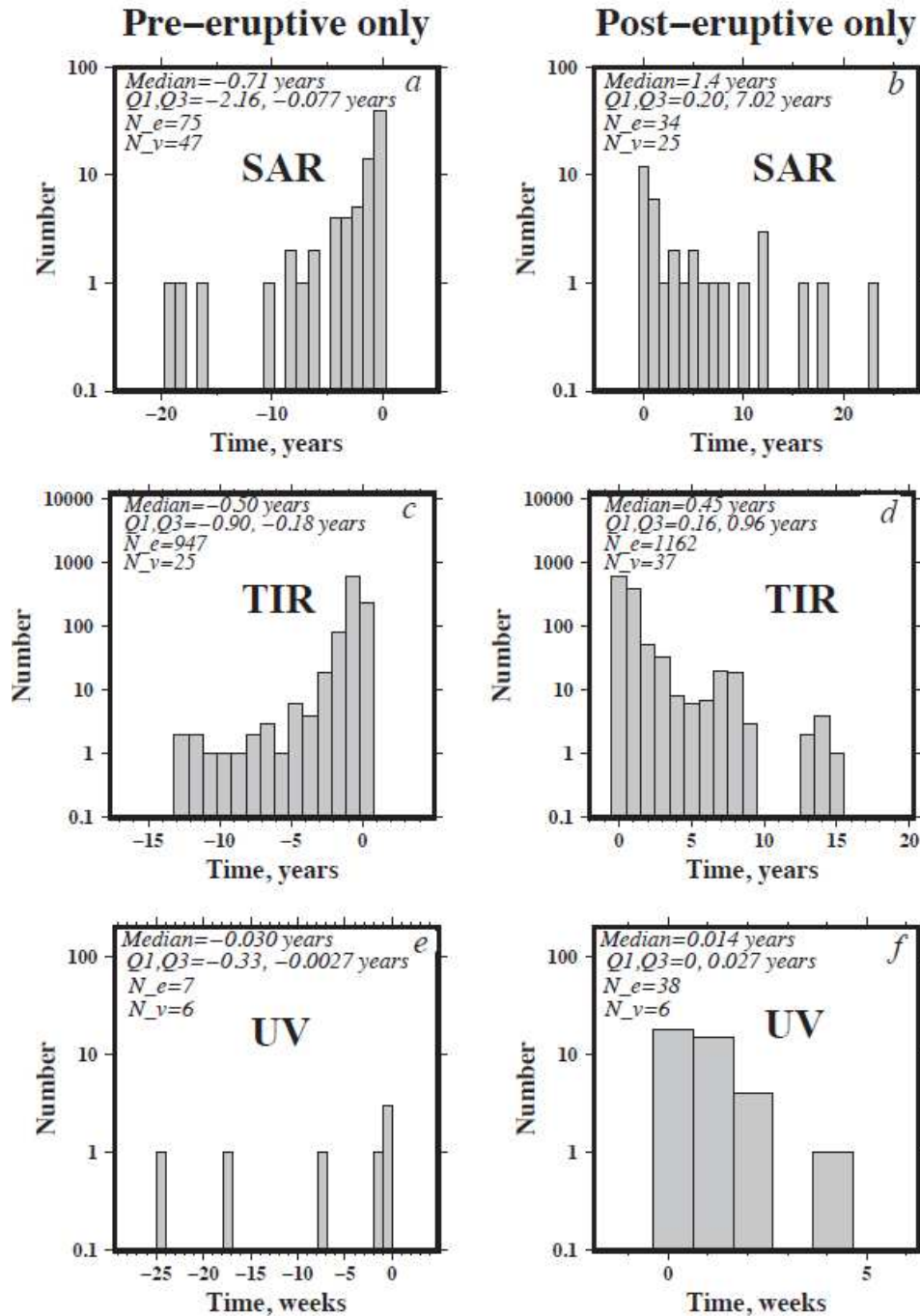


Figure 9. Time between satellite-detections from each sensor and eruption (Global Volcanism Program, 2013). The left column shows only pre-eruptive detections while the right column shows only post-eruptive detections. Figures 9a and 9b show satellite-detected deformation from SAR sensors, Figures 9c and 9d show satellite-detected thermal features from TIR sensors, and Figures 9e and 9f show satellite-detected SO₂ degassing from UV sensors. The shorthand “N_e” stands for number of episodes, “N_v” stands for number of volcanoes, and “Q1” and “Q3” refer to the first and third quartile, respectively.

calculate for SAR and TIR may be better classified as non-eruptive satellite-detections. For TIR our timing database is composed of MODVOLC data, and for satellite-detected thermal features to be measured both years before and years after an eruption points to persistently active volcanoes (with repose periods of at least a few years, e.g. Bezmianny (Russia) or Nyamuragira (Democratic Republic of the Congo)) or volcanoes with fumarole activity or missing information on eruptions (e.g. Momotombo (Nicaragua) and Gamkonora (Indonesia)). For SAR, the lengthy post-eruptive period may also relate to persistently active volcanoes though the lengthy pre-eruptive period is consistent with other studies. Biggs and Pritchard (2017) showed deformation events lasting on the order of decades that were related to eruptions. We also compare our results with a study dominated by ground-based data (Phillipson et al., 2013, see Table 3). The Phillipson et al. (2013) study analyzed ten years of activity reports (2000-2011) from the Global Volcanism Program (which was principally ground-based data at the time) and reported durations of pre-eruptive detections based on instrument type and volcano type. Their study suggests that deformation (N=27 episodes) occurred a mean of 1001 days before an eruption, thermal features (N=32) occurred a mean of 36 days before an eruption, and degassing (N=59) occurred a mean of 341 days before an eruption (Phillipson et al., 2013). The means of our pre-eruptive data for deformation, thermal features, and SO₂ degassing are: 797 days, 274 days, and 51 days, respectively. The Phillipson et al. (2013) results for deformation are similar to ours whereas the results for thermal features and degassing are fairly different. However, both studies involve relatively small sample sizes with large standard deviations. We question the pre-eruptive timing of thermal features from our study given that the MODVOLC algorithm primarily captures eruptive activity. The measurement method of thermal features in the Phillipson et al. (2013) study does include some hot spots from remote sensing but additionally

includes ground-based measurements of changes in fumarole temperature. Their timing of 36 days prior to an eruption is more consistent with case studies in which pre-eruptive thermal features were measured by ASTER in the months preceding an eruption. For SO₂ degassing, our database is dominated by eruptive measurements of degassing and includes only a few instances of pre-eruptive measurements while the Phillipson et al. (2013) study includes more episodes. Further, ground-based measurements of degassing are more sensitive to the emission of CO₂ (which usually occurs before SO₂) and to shifts from hydrothermal to magmatic compositions (i.e. water-rich to CO₂ rich, increasing ³He/⁴He) in fumaroles. The satellite sensors are so far mostly restricted to measurement of SO₂ which exsolves relatively shallow, hence this bias towards later detection of SO₂ might be expected from the current satellite record.

Description	Deformation (our study, pre-eruptive)	Deformation (Phillipson et al., 2013)	Thermal (our study, pre-eruptive)	Thermal (Phillipson et al., 2013)	SO ₂ (our study, pre-eruptive)	SO ₂ (Phillipson et al., 2013)
# episodes	75	27	947	32	7	59
# volcanoes	47	n/a	25	n/a	6	n/a
Mean	-797 (days)	-1001 (days)	-274 (days)	-36 (days)	-51 (days)	-341 (days)
Median	-260 (days)	-239 (days)	-184 (days)	-6 (days)	-11 (days)	-30 (days)
Mode	-38 (days)	n/a	-29 (days)	n/a	-1 (days)	n/a
Standard dev.	1453 (days)	1558 (days)	440 (days)	78 (days)	69 (days)	1358 (days)
Min value	-7027 (days)	-5755 (days)	-4625 (days)	-1 (days)	-171 (days)	-9830 (days)
Max value	-2 (days)	-2 (days)	-1 (days)	-377 (days)	-1 (days)	-1 (days)

Table 3. Timing between satellite-detections and eruptions for pre-eruptive detections (data are displayed in Figure 9). This is compared against a similar study of dominantly ground-based measurements of unrest by Phillipson et al., 2013.

4.2 Differences by volcano type

Further, Phillipson et al. (2013) found that pre-eruptive unrest duration is related to volcano type. They suggest that non-eruptive unrest is often longer lasting (median duration 227 days) than pre-eruptive unrest (median duration 60 days), and that duration of unrest is shortest for complex volcanoes (median duration 2 days). Passarelli and Brodsky (2012) also note that run-

up time (duration between pre-eruptive detections and eruption) correlates positively with repose time (timing between eruptions), as well as with increasing SiO₂ content. Biggs and Pritchard (2017) compared durations of 485 deformation events for 221 volcanoes to eruptions or lack thereof, and determined that shorter lasting deformation events (duration of < 1 year) of large magnitude (> 10² mm/year) often lead to eruption, though there is no simple threshold in duration or magnitude.

Diversity in magma composition, volcano type, and tectonic setting has clear implications for the presence (and measurement) of volcanic activity. In the case of magmatic deformation, the deformation expression and magnitude are related to volatile content and magma compressibility, magma supply, and the depth of magma storage (e.g. Johnson et al., 2000; Hautmann et al., 2010; Voight et al., 2010). Magmatic deformation is less likely to be measured in areas with deep magma chambers (e.g. Chaussard et al., 2013; Grapenthin et al., 2013; Ebmeier et al., 2013, Pritchard and Simons, 2002), in cases where magmas exhibit high exsolved volatile contents (rendering them more compressible, e.g. Johnson, 1992; Mastin et al., 2008; McCormick Kilbride et al., 2016), or for magmas which may rise quickly without coupling to the surrounding country rock (e.g. Dzurisin et al., 2008; Ebmeier et al., 2013). For such instances where deformation is unlikely to be measured, measurements of volcanic degassing or thermal surveys may prove more fruitful for monitoring volcanic activity (e.g. Moran et al., 2006).

Measurements of volcano SO₂ degassing by satellite, in contrast, are dependent upon the detection limits described in previous sections (involving plume altitudes, season, and latitude), but will also vary with magmatic SO₂ content, redox state, interaction with other gases, and the ability of SO₂ to accumulate at the top of a magma reservoir (e.g. McCormick Kilbride et al.,

2016). Remote sensing of volcanic gases exhibit significant biases for volcanoes in tropical settings due to the aforementioned challenges for UV/VIS remote sensing spectroscopy at extreme latitudes (e.g. McCormick et al., 2013). Satellite limitations aside, volcanic SO₂ output may be thwarted by interaction with hydrothermal systems or surficial ice which “scrub” the magmatic gases (e.g. Werner et al., 2011; Theys et al., 2013), and, as already mentioned, the emission of SO₂ is often delayed relative to the emission of CO₂. Therefore this type of monitoring may not be best for some volcanoes, especially during the pre-eruptive period (e.g. Symonds et al., 2001).

It follows that there are volcanoes where detection limits will never permit measurement from multiple types of satellite sensors. Instead, having these varied types of sensors conducting measurements is likely necessary to capture the inherent diversity in volcanic activity. The multi-sensor, multi-satellite method detected volcanic activity at more volcanoes than any of the sensors can measure alone (see Figure 14), and notable geographic patterns are delineated from this analysis. Thermal feature detections are concentrated in South America and Antarctica, probably because we include observations from dedicated thermal surveys of these regions (South America: Jay et al., 2015; Antarctica: Patrick and Smellie, 2013). Measurements of SO₂ degassing are particularly common in Indonesia and Central America, consistent with analysis of solely TOMS-based measurements conducted by Carn et al., (2003), as these areas include higher proportions of recently erupting volcanoes that are more favorable for detection and the detection limits of the sensors are lower for these low-latitude emissions. Measurements of deformation are more globally widespread, owing partially to the existence of many regional deformation surveys (e.g. South America and Kamchatka: Pritchard and Simons, 2004; Central America: Ebmeier et al., 2013; Alaska and Aleutians: Lu and Dzurisin, 2014; Mexico and

Indonesia: Chaussard et al., 2013; Iceland: Sigmundsson, 2006; Africa: Biggs et al., 2009, Biggs et al., 2011) coupled with the distinct all-weather, day/night operability of SAR sensors (e.g. Lu, 2007). However, there are also regions notably absent from all our “global” datasets, especially InSAR, because systematic global coverage and analysis has not yet been undertaken. For example, tropical settings exhibit dense vegetation and high atmospheric water vapor which poses a challenge to SAR measurements such that these areas have been understudied (Pyle et al., 2013). Tropical areas are also best studied using longer wavelengths, like L-band, though the record of L-band sensors is shortest (see Table 1).

Certainly, these regional biases are not entirely divorced from variation in satellite spatial and temporal sampling, though additional regional discrepancy in volcanic activity may also be significant. The next decades of research and incorporation of all available satellite data will allow us to determine whether regional differences are related to differences in the frequency and character of volcanic activity or measurement resolution limitations. Nonetheless, as a direct result of this compilation, 306 unique volcanoes had detections from at least one type of satellite sensor. We do not mean to imply that other methods (other satellite methods or other ground-based methods) could not measure activity at these volcanoes; rather we mean to emphasize the breadth and utility of satellite remote-sensing for applications to volcanology research.

4.3 Recommendations for future satellite monitoring

For thermal sensors, cloud coverage obstructs observations of Earth’s surface and limits the number of usable images for many volcanoes (e.g. Rothery et al., 1988). In theory, between 2000-2016 a non-prioritized volcano should have been observed with ASTER approximately 350 times [$((365 \text{ days in a year} / \text{one image nominally every 16 days})) * 16 \text{ years of observation}$]. Though the volcanoes we surveyed had four to 203 usable ASTER images between 2000-2016

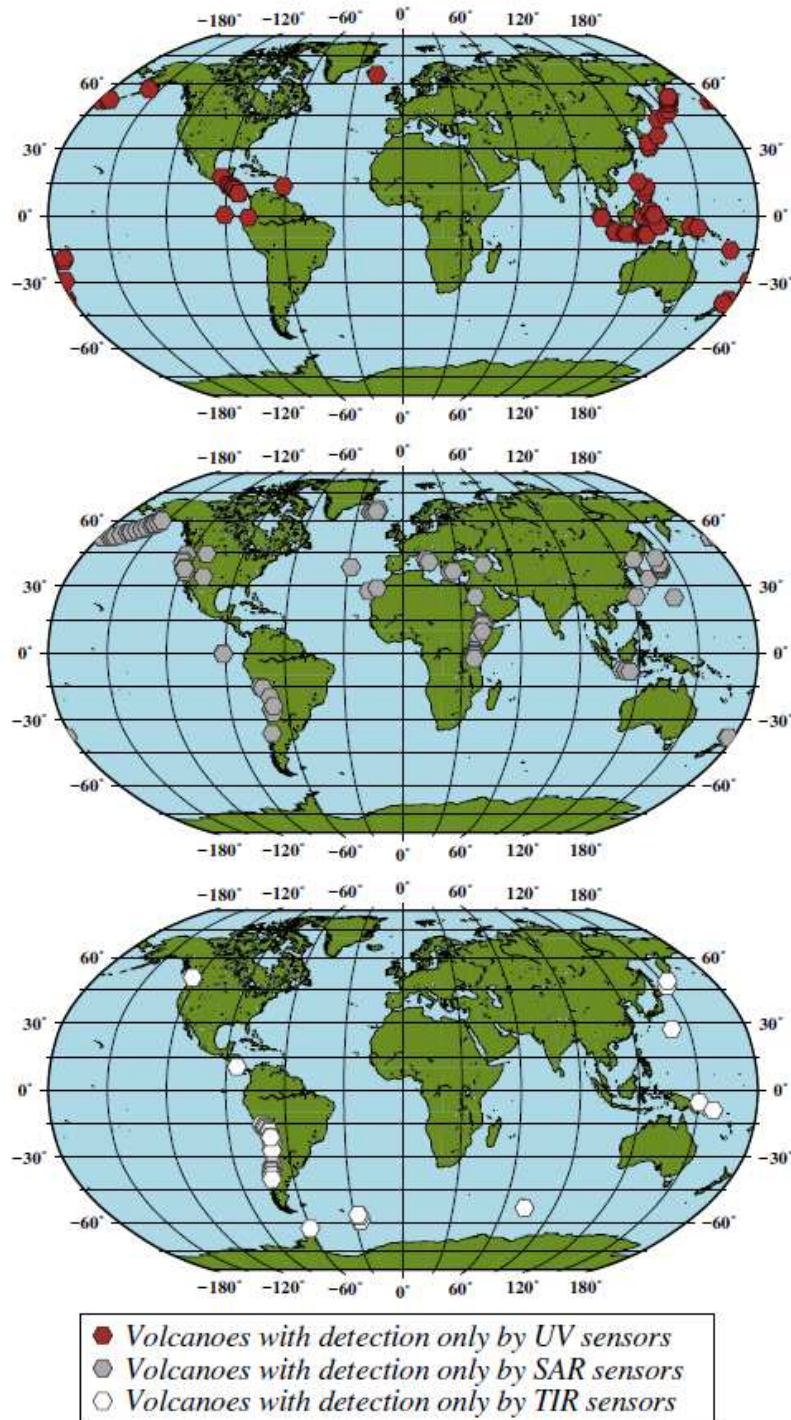


Figure 14. Volcanoes plotted with satellite-detections colored according to method of detection. Maroon hexagons (top) represent volcanoes with unique detection by TIR sensors (N=45), grey hexagons (middle) represent volcanoes with unique detection by SAR sensors (N=86), and white hexagons (bottom) represent volcanoes uniquely detected by UV/VIS sensors (N=59). The spatial patterns of detection are described in the main text.

with many volcanoes exhibiting gaps in usable data that can span years. Similarly, a multi-year eruption at El Reventador (Ecuador) was captured repeatedly by MODVOLC but only two of the 136 ASTER images of the area were free of cloud coverage (Naranjo et al., 2016). As such, the shortage of satellite detections from TIR sensors at these volcanoes may stem from persistent cloud coverage or eruptions of short duration or low-intensity. For example, neither MODVOLC nor ASTER could detect a minor eruption at Marion Island (Southern Ocean) probably due to the short duration of the eruption (Patrick and Smellie, 2013).

However, the 14 volcanoes we found to be detectable with ASTER but not MODVOLC (described in section 3.2) underline the importance of using multiple data types, and multiple sensor resolutions, to capture various types of volcanic activity. Jay et al. (2013) surveyed 150 volcanoes in the central and southern Andes using both MODVOLC and ASTER and found 35 volcanic areas with thermal features detected with ASTER and six volcanic areas with thermal features detected with MODVOLC. The six volcanic areas found with MODVOLC were also identified using ASTER, though the two were not always concurrent. Additionally, Jay et al. (2013) found that MODVOLC captured mostly eruptive episodes while ASTER thermal features resulted from fumaroles and geothermal systems. In five volcanic areas with sufficient ASTER temporal resolution, the temperature of the thermal features correlated with known eruptive activity and this trend was observable in the months or years leading to eruption.

Owing to variation in temporal and spatial resolution of each thermal sensor, our focus on few sensors here does not capture the full capability of all thermal sensors. For example, the thermal sensors discussed here utilize polar orbits with daily repeat intervals though thermal sensors on geostationary orbits with repeat intervals of minutes to hours have also been useful to

detect thermal features before and during an eruption (e.g. SEVIRI: Ganci et al., 2011, Corradini et al., 2018, AVHRR: Pergola et al., 2004).

The advantages of the evolution of sensor capabilities combined with the concurrent deployment of sensors with contrasting spatial and temporal resolutions can also be seen with SAR. The recent high-resolution satellite constellation of COSMO-SkyMed SAR sensors detected deformation missed by the contemporaneous SAR sensors Envisat and Sentinel (e.g. Stephens et al., 2017; Hamling et al. 2016). Repeated observations of the same volcano with sensors exhibiting different spatiotemporal resolutions can improve characterization of deformation events like at Colima volcano (Mexico), where initial observations with C-band sensors detected deformation (in 2004, Pinel et al., 2011) but observations with X-band sensors revealed more extensive deformation (in 2013, Salzer et al., 2014).

For those volcanoes that erupt and do not have any type of satellite-detection, perhaps satellite passes occur too infrequently or have insufficient resolution for detecting activity of small magnitude and small spatial extent. Seismic and other ground-based methods may be better suited to detecting volcanic activity prior to low-magnitude eruptions or eruptions with short run-up times. In large part, eruptions at these volcanoes without satellite-detections did not display any activity or did not display activity that could have been detected by satellite (i.e. seismicity). For those that produced fumaroles and steam emissions, we suspect that these were of low magnitude (to produce low VEI eruptions), and produced a thermal output below the capability of the satellite sensors considered here. Furthermore, the majority of volcanoes with eruptions since 1978 did have some form of activity detected by the satellite sensors. Nonetheless, there is a clear need for more satellite sensors that observe globally over volcanoes—especially for volcanic thermal features—in order to capture the full diversity in types of volcanic activity, a

full spectrum from spatially extensive and high-magnitude features to spatially restricted, lower-magnitude features.

Of course, there are volcanoes that cannot be easily monitored by satellite. For example, certain small volcanic islands can be difficult to survey using sensors with larger pixel sizes. Thermal features at White Island have never been detected by the MODVOLC algorithm utilizing MODIS sensors (at 1 km/pixel) but were easily observable with ASTER imagery (at 90 m/pixel, see Figure 15), and from ground-based methods (e.g. Global Volcanism Program, 2013). For those volcanoes with a known history of only low-VEI eruptions, short time periods between detection and eruption, and for generally smaller volcanoes, ground-based data are potentially the only way to detect activity. Satellite observations could provide additional guidance in these cases if they were to primarily consist of sensors with high spatial resolutions. As higher spatial resolutions often compromise satellite observation frequency, it may be necessary to deploy multiple satellites of higher spatial resolution which operate in coordination (i.e. COSMO-SkyMed, and future proposed constellations, e.g. Grandoni et al., 2014; Milillo et al., 2016) such that the volcano is surveyed every few days, if not more frequently. While we have demonstrated that the high-resolution ASTER data can measure thermal features at volcanoes that produce low magnitude eruptions (Figure 15, and supplementary Figures 1-11), it is not yet possible to define timings between thermal features and eruption on a global scale with the current data available. This could be improved with an accurate global database of the available ASTER data and the inclusion of multiple high-resolution satellites that capture more precursory activity. Such a system would also greatly improve understanding of timing between volcanic activity and eruption since eruptions are often more frequent at volcanoes which produce lower-VEI eruptions (e.g. Passarelli and Brodsky, 2012).

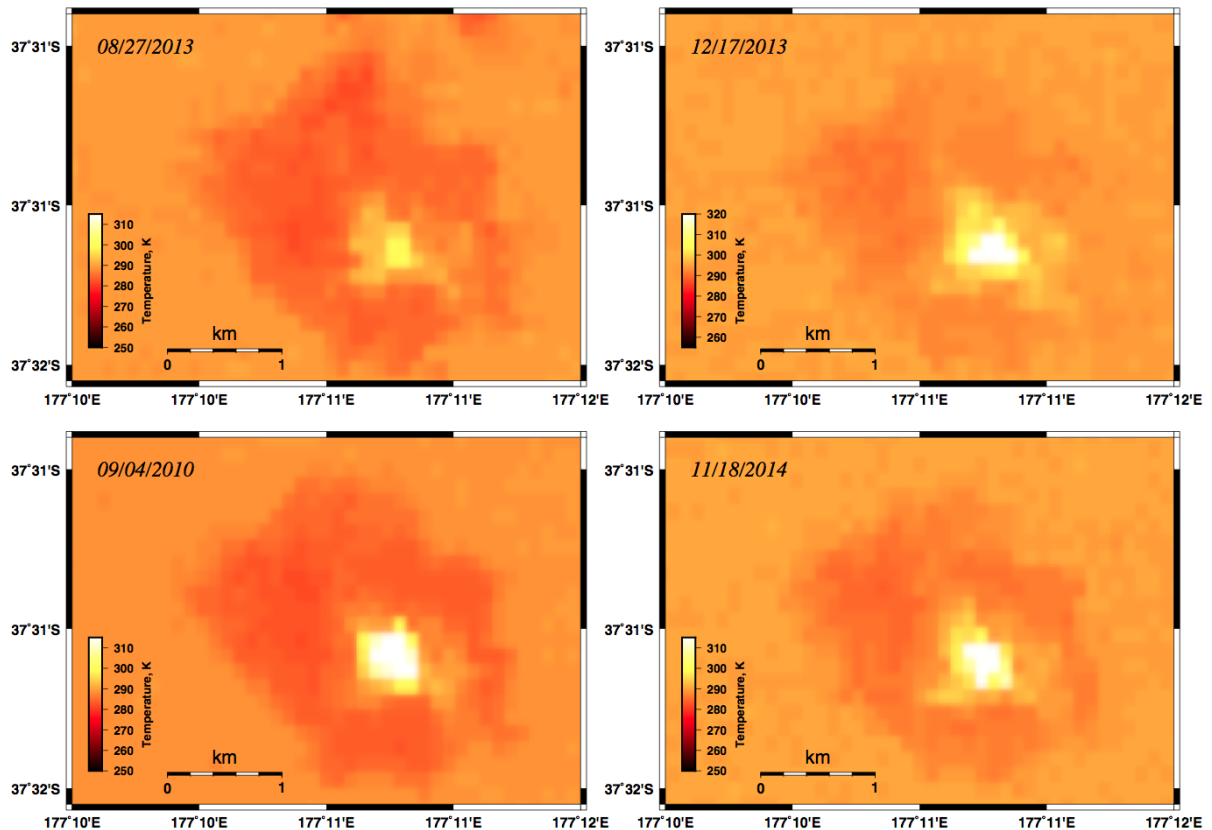


Figure 15. Selected ASTER images showing potential thermal features at White Island volcano. Anomalous pixels are at least 10 K above background temperatures.

5. Conclusions

We have shown how satellite measurements have contributed to volcano research in the past few decades, providing observations of deformation, SO_2 degassing, and thermal features at volcanoes, some of which were not otherwise monitored. This multi-sensor, multi-satellite approach includes detection for at least 306 volcanoes worldwide, with satellite detection indicating a higher likelihood for eruption over the standard eruption rate (the null hypothesis). There have been many more volcanoes where satellite measurement has occurred though nothing was detected, although we do not yet have a robust database of null results. Having global,

continuously updated records of satellite-detected volcanic activities or lack thereof may be particularly useful in the future for delineating zones of volcanic hazard.

We have compiled and integrated global databases of volcanic activity measured by three satellite-based techniques: SAR, TIR, and UV/VIS spectroscopy over the past few decades. Because this is the first multi-sensor and global comparison, we caution that our results are still preliminary. We note patterns in volcanic activity occurring worldwide, namely that activity is occurring at volcanoes generally not thought to be active. We note that satellite sensors have detected activity at the majority of volcanoes that experienced eruptions between 1978-2016 (78%), suggesting that satellite sensors are a capable tool in this regard. We calculate a statistically significant association between satellite-detection and eruption and those volcanoes that do not erupt and also do not have a satellite-detection. Despite the uncertainties in start and end dates of eruptions and satellite-detected activities, satellites are successfully identifying eruptions and the most active volcanoes worldwide. Volcanoes with recent eruption that were missed by the satellite sensors in our database are likely related to the more limited resolutions and higher detection thresholds of the earlier generations of sensors, as well as the shorter lifespan of the SAR and TIR sensors. Our analysis of ASTER data for a subset of volcanoes with recent eruption without satellite-detection indicates that the improved resolution and detection threshold of ASTER over MODIS could indeed supplement our database of satellite-detections and shorten our list of “missed” eruptions (supplementary Tables 10, 11 and supplementary Figures 1-11).

Volcanoes with detection by multiple sensors are more closely associated with eruptions (i.e., 44% for one type of sensor vs. 98% for three types). This is to be expected given that our UV and TIR databases predominantly measured co-eruptive activity. As these databases grow to

include more detailed passive SO₂ emissions and ASTER data as well as other high spatial and temporal resolution sensors, we suspect that a more informative comparison of timing between satellite-detections and eruption will emerge. For now, each of these sensors has provided an important role in enhancing our knowledge of active volcanism worldwide (i.e. unique detections of volcanic activity not seen by other sensors). We have also supplemented previous work to show that deformation may occur months before an impending eruption.

Ultimately, satellite-detected activities are not simple to interpret. In most cases, satellite-detections are not followed by an immediate eruption (e.g. Biggs et al., 2014; Potter et al., 2015, and the latest results from our study). We do not find any simple relationship between eruption and type of satellite-detection, which would suggest that volcanoes produce unique activity prior to eruption. Yet we must be cautious in this interpretation as the duration of multi-sensor satellite coverage has been short relative to eruption cycle timescales, and spatial coverage is not universally of sufficient resolution to detect volcanic activity.

Though the global analysis of multiple satellite datasets is still in its infancy, we hope that community involvement and support can sustain and expand these datasets. Even a simple integration of these datasets can relate types of volcanoes and volcanic settings to satellite-detections, allowing better insight into volcanic reactivation. We look forward to the next few decades with promises of more satellite missions, as well as to the commitment within the volcanological community to create more integrated and comprehensive databases of volcanic activity.

Acknowledgments

We thank Robert Wright for critical insight in creating our thermal database, David Furtney for programming expertise and code review, Daniel Portner and William J. Durkin for assistance with figures, and two anonymous reviewers for their thoughtful commentary that

greatly improved this manuscript. The Generic Mapping Tools program was used to make several figures (Wessel et al., 2013). M.A.F. and M.E.P. were partially supported by NASA's Science Mission Directorate grants NNX12AM24G, NNX12AO31G, and NNX16AK87G. J.A.J. was supported by NASA grant NNX12AM24G and the Smithsonian Institution Global Volcanism Program postdoctoral fellowship. K.A.R. was supported by NASA grant NNX16AK87G and the Volcano Remote Sensing Working Group supported by the John Wesley Powell Center for Analysis and Synthesis, funded in part by the U.S. Geological Survey. BTMK acknowledges funding from the Centre for Observation and Modeling of Earthquakes, Volcanoes and Tectonics (COMET). S.K.E. is funded by a Leverhulme Early Career Fellowship and a European Space Agency fellowship, which was formerly held at the University of Bristol and co-funded by COMET. J.B. is funded by COMET and by NERC grant STREVA (NE/J020052/1).

[1]
[SEP]

References

- Abrams, M. (2000), The Advanced Spaceborne Thermal Emission and Reflection Radiometer (ASTER): Data products for the high spatial resolution imager on NASA's Terra platform, *International Journal of Remote Sensing*, 21(5), 847–859, doi: 10.1080/014311600210326.
- Abrams, M., S. Hook, and B. Ramachandran (2004), *ASTER User Handbook*, 2, Jet Propulsion Laboratory, California Institute of Technology.
- Baer, G., Y. Hamiel, G. Shamir, and R. Nof (2008), Evolution of a magma-driven earthquake swarm and triggering of the nearby Oldoinyo Lengai eruption, as resolved by InSAR, ground observations and elastic modeling, *East African Rift, 2007*, *Earth and Planetary Science Letters*, 272, 339–352, doi: 10.1016/j.epsl.2008.04.052.
- Bani, P., Oppenheimer, C., Allard, P., Shinohara, H., Tsanev, V., Carn, S., Lardy, M., and E. Garaebiti (2012), First estimate of volcanoc SO₂ budget for Vanuatu island arc, *Journal of Volcanology and Geothermal Research*, 211–212, p. 36–46, doi: 10.1016/j.jvolgeores.2011.10.005.
- Barberi, F., R. Blong, S. de la Cruz, M. Hall, K. Kamo, P. Mothes, C. Newhall, D. Peterson, R. Punongbayan, G. Sigvadason, and N. Zana (1990), Reducing volcanic disasters in the 1990s, *Bulletin of the Volcanological Society of Japan*, 35(1), 80–95.
- Begeuría, S. (2006), Validation and evaluation of predictive models in hazard assessment and risk management, *Natural Hazards*, 37(3), 315–329, doi: 10.1007/s11069-005-5182-6.
- Berresheim, H. and W. Jaeschke (1983), The contribution of volcanoes to the global atmospheric sulfur budget, *Journal of Geophysical Research*, 88(C6), 3732–3740.
- Biggs, J., E.Y. Anthony, and C.J. Ebinger (2009), Multiple inflation and deflation events at Kenyan volcanoes, *East African Rift*, *Geology*, 37(11), doi: 10.1130/G30133A.1.

Biggs, J., I.D. Bastow, D. Keir, and E. Lewi (2011), Pulses of deformation reveal frequently recurring shallow magmatic activity beneath the Main Ethiopian Rift, *Geochemistry, Geophysics, Geosystems*, 12, doi: 10.1029/2011GC003662.

Biggs, J., S.K. Ebmeier, W.P. Aspinall, Z. Lu, M.E. Pritchard, R.S.J. Sparks, and T.A. Mather (2014), Global link between deformation and volcanic eruption quantified by satellite imagery, *Nature Communications*, 5, doi: 10.1038/ncomms4471.

Biggs, J. and M.E. Pritchard (2017), Global volcano monitoring: What does it mean when volcanoes deform?, *Elements*, 13, 17-22, doi: 10.2113/gselements.13.1.17.

Bignami C., Corradini S., Merucci L., de Michele M., Raucoules D., Stramondo S., Piedra J., “Multi-sensor satellite monitoring of the 2011 Puyheue-Cordon Caulle Eruption”, *JSTARS*-2014-00089, 7(7), doi: 10.1109/JSTARS.2014.2320638.

Bluth, G.J.S., S.D. Doiron, C.C. Schnetzler, A.J. Krueger, and L.S. Walter (1992), Global tracking of the SO₂ clouds from the June, 1991 Mount Pinatubo eruptions, *Geophysical Research Letters*, 19(2), doi: 10.1029/91GL02792.

Bonneville, A., G. Vasseur, and Y. Kerr (1985), Satellite thermal infrared observations of Mt. Etna after the 17th March 1981 eruption, *Journal of Volcanology and Geothermal Research*, 24, doi: 10.1016/0377-0273(85)90074-5.

Bonneville, A. and Y. Kerr (1987), A thermal forerunner of the 28th March 1983 Mt. Etna eruption from satellite thermal infrared data, *Journal of Geodynamics*, 7(1-2), doi: 10.1016/0264-3707(87)90061-5.

Brown, S.K., M.R. Auken, and R.S.J. Sparks (2015a), Populations around Holocene volcanoes and development of a Population Exposure Index, In: Loughlin, S.C., S. Sparks, S.K. Brown, S.F. Jenkins, and C. Vye-Brown (eds.), *Global Volcanic Hazards and Risk*, Cambridge University Press, Cambridge, in press.

Brown, S.K., S.C. Loughlin, R.S.J. Sparks, C. Vye-Brown, J. Barclay, E. Calder, E. Cottrell, G. Jolly, J-C. Komorowski, C. Mandeville, C. Newhall, J. Palma, S. Potter, G. Valentine, B. Baptie, J. Biggs, H.S. Crossweller, E. Ilyinskaya, C. Kilburn, K. Mee, and M. Pritchard (2015b), Global volcanic hazard and risk, In: Loughlin, S.C., S. Sparks, S.K. Brown, S.F. Jenkins, and C. Vye-Brown (eds.), *Global Volcanic Hazards and Risk*, Cambridge University Press, Cambridge, in press.

Campion, R., Salerno, G.G., Coheur, P.-F., Hurtmans, D., Clarisse, L., Kazahaya, K., Burton, M., Caltabiano, T., Clerbaux, C., and A. Bernard (2010), Measuring volcanic degassing of SO₂ in the lower troposphere with ASTER band ratios, *Journal of Volcanology and Geothermal Research*, 194(1-3), p. 42-54, doi: 10.1016/j.jvolgeores.2010.04.010.

Campion, R. (2014), New lava lake at Nyamuragira volcano revealed by combined ASTER and OMI SO₂ measurements, *Geophysical Research Letters*, 41(21), 7485–7492, doi: 10.1002/2014GL061808.

Carn, S.A. (2015), Multi-Satellite Volcanic Sulfur Dioxide L4 Long-Term Global Database V2, version 2, Greenbelt, MD, USA, Goddard Earth Science Data and Information Services Center (GES DISC), accessed April 2016, <ftp://measures.gsfc.nasa.gov/data/s4pa/SO2/MSVOLSO2L4.2/>

Carn, S.A., Clarisse, L., and Prata, A.J. (2016), Multi-decadal satellite measurements of global volcanic degassing, *Journal of Volcanology and Geothermal Research*, 311, 99–134, doi: 10.1016/j.jvolgeores.2016.01.002.

Carn, S.A., V.E. Fioletov, C.A. McLinden, C. Li, and N.A. Krotkov (2017), A decade of global volcanic SO₂ emissions measured from space, *Scientific Reports*, 7, doi: 10.1038/srep44095.

Carn, S.A., Krotkov, N.A., Yang, K., and Krueger, A.J. (2013), Measuring global volcanic degassing with the Ozone Monitoring Instrument (OMI), Geological Society, London, Special Publications, 380(1), 229–257, doi: 10.1144/SP380.12.

Carn, S.A., Krueger, A.J., Arellano, S., Krotkov, N.A., and Yang, K., (2008), Daily monitoring of Ecuadorian volcanic degassing from space, *Journal of Volcanology and Geothermal Research*, 176(1), 141-150.

Carn, S.A., Krueger, A.J., Bluth, G.J.S., Schaefer, S.J., Krotkov, N.A., Watson, I.M., and Datta, S., (2003), Volcanic eruption detection by the Total Ozone Mapping Spectrometer (TOMS) instruments: A 22-year record of sulphur dioxide and ash emissions, Geological Society, London, Special Publications, 213(1), 177–202, doi: 10.1144/GSL.SP.2003.213.01.11.

Carn, S.A., Krueger, A.J., Krotkov, N.A., Yang, K., and Evans, K., (2009a), Tracking volcanic sulfur dioxide clouds for aviation hazard mitigation, *Natural Hazards*, 51(2), 325–343, doi: 10.1007/s11069-008-9228-4.

Carn, S.A., J.S. Pallister, L. Lara, J.W. Ewert, S. Watt, A.J. Prata, R.J. Thomas, and G. Villarosa (2009b), The unexpected awakening of Chaiten volcano, Chile, *EOS*, 90(24), doi: 10.1029/2009EO240001.

Cashman, K. and J. Biggs, (2014), Common processes at unique volcanoes-a volcanological conundrum, *Frontiers in Earth Science*, 2(28), 1-4, doi: 10.3389/feart.2014.00028.

Chaussard, E., F. Amelung, and Y. Aoki (2013), Characterization of open and closed volcanic systems in Indonesia and Mexico using InSAR time series, *Journal of Geophysical Research*, 118(8), doi: 10.1002/jgrb.50288.

Chaussard, E., S. Wdowinski, E. Cabral-Cano, and F. Amelung (2014), Land subsidence in central Mexico detected by ALOS InSAR time-series, *Remote Sensing of Environment*, 140, doi: 10.1016/j.rse.2013.08.038.

Coppola, D., M. Laiolo, and C. Cigolini (2016a), Fifteen years of thermal activity at Vanuatu's volcanoes (2000-2015) revealed by MIROVA, *Journal of Volcanology and Geothermal Research*, 322, doi: 10.1016/j.jvolgeores.2015.11.005.

Coppola, D., M. Laiolo, C. Cigolini, D. Delle Donne, and M. Ripepe (2016b), Enhanced volcanic hot-spot detection using MODIS IR data: results from the MIROVA system, In: Harris, A.J.L., T. De Groeve, F. Garel, and S.A. Carn (eds.), *Detecting, Modelling and Responding to Effusive Eruptions*, Geological Society, London, Special Publications, 426, 181-205, doi: 10.1144/SP426.5.

Corradini, S., L. Guerrieri, V. Lombardo, L. Merucci, M. Musacchio, M. Prestifilippo, S. Scollo, M. Silvestri, G. Spata, and D. Stelitano (2018), Proximal monitoring of the 2011-2015 Etna lava fountains using MSG-SEVIRI data, *Geosciences*, 8(140), doi: 10.3390/geosciences8040140.

Corradini, S., L. Merucci, A.J. Prata, and A. Piscini, (2010), Volcanic ash and SO₂ in the 2008 Kasatochi eruption: Retrievals comparison from different IR satellite sensors, *Journal of Geophysical Research*, 115(D2), doi: 10.1029/2009JD013634.

Dean, K., J. Dehn, S. McNutt, C. Neal, R. Moore, and D. Schneider (2002), Satellite imagery proves essential for monitoring erupting Aleutian volcano, *EOS*, 83(22), 241-247, doi: 10.1029/2002EO000168.

Delgado, F., Pritchard, M., Lohman, R., and Naranjo, J.A., (2014), The 2011 Hudson volcano eruption (Southern Andes, Chile): Pre-eruptive inflation and hotspots observed with InSAR and thermal imagery, *Bulletin of Volcanology*, 76(5), doi: 10.1007/s00445-014-0815-9.

Delle Donne, D., Harris, A.J., Ripepe, M., and Wright, R., (2010), Earthquake-induced thermal anomalies at active volcanoes, *Geology*, 38(9), 771-774, doi: 10.1130/G30984.1.

Ding, X., Z. Li, J. Zhu, G. Feng, and J. Long (2008), Atmospheric effects on InSAR measurements and their mitigation, *Sensors*, 8(9), doi: 10.3390/s8095426.

Dzurisin, D., M. Lisowski, M.P. Poland, D.R. Sherrod, and R.G. LaHusen, (2008), Constraints and conundrums resulting from ground-deformation measurements made during the 2004-2005 dome-building eruption of Mount St. Helens, Washington, In: Sherrod, D.R., W.E. Scott, and P.H. Stauffer (eds.), *A Volcano Rekindled: The Renewed Eruption of Mount St. Helens, 2004-2006*, U.S. Geological Survey Professional Paper 1750, 281-300.

Ebmeier, S.K., B.J. Andrews, M.C. Araya, D.W.D. Arnold, J. Biggs, C. Cooper, E. Cottrell, M. Furtney, J. Hickey, J. Jay, R. Lloyd, A.L. Parker, M.E. Pritchard, E. Robertson, E. Venzke, and J.L. Williamson (2018), Synthesis of global satellite observations of magmatic and volcanic

deformation: implications for volcano monitoring & the lateral extent of magmatic domains, *Journal of Applied Volcanology*, 7(2), doi: 10.1186/s13617-018-0071-3.

Ebmeier, S.K., Biggs, J., Mather, T.A., and Amelung, F., (2013), On the lack of InSAR observations of magmatic deformation at Central American volcanoes: InSAR measurements of the CAVA, *Journal of Geophysical Research: Solid Earth*, 118(5), 2571–2585, doi: 10.1002/jgrb.50195.

Ewert, J.W. (2007), System for ranking relative threats of U.S. Volcanoes, *Natural Hazards Review*, 8(4), 112-124, doi: 10.1061/(ASCE)1527-6988(2007)8:4(112).

Ferrucci, F., F. Prata, F. Amelung, G. Bawden, J. Biggs, P. Briole, C. Del Negro, M. Eineder, C. Jordan, S. Loughlin, G. Puglisi, M. Bianchi, S. Tait, N. Theys, D. Schneider, and D. Norbury (2012), Perspectives concerning satellite EO and geohazard risk management: volcanic hazards, In: Bally, P. (ed), *The International Forum on Satellite EO and Geohazards, The Santorini Conference, 21-23 May 2012, Santorini, Greece, European Space Agency*, doi: 10.5270/esa-geo-hzrd-2012.

Fioletov, V.E., C.A. McLinden, N. Krotkov, C. Li, J. Joiner, N. Theys, S. Carn, and M.D. Doran (2016), A global catalogue of large SO₂ sources and emissions derived from the Ozone Monitoring Instrument, *Atmospheric Chemistry and Physics*, 16(18), doi: 10.5194/acp-16-11497-2016.

Foster, J., B. Brooks, T. Cherubini, C. Shacat, S. Businger, and C.L. Werner (2006), Mitigating atmospheric noise for InSAR using a high resolution weather model, *Geophysical Research Letters*, 33(16), doi: 10.1029/2006GL026781.

Fournier, T.J., Pritchard, M.E., and Riddick, S.N., (2010), Duration, magnitude, and frequency of subaerial volcano deformation events: New results from Latin America using InSAR and a global synthesis, *Geochemistry, Geophysics, Geosystems*, 11(1), 1-29, doi: 10.1029/2009GC002558.

Francis, P.W. and S.L. De Silva, (1989), Application of the Landsat Thematic Mapper of the identification of potentially active volcanoes in the Central Andes, *Remote Sensing of Environment*, 28, 245-255, doi: 10.1016/0034-4257(89)90117-X.

Francis, P.W. and D.A. Rothery, (1987), Using the Landsat Thematic Mapper to detect and monitor active volcanoes: An example from Lascar volcano, northern Chile, *Geology*, 15(7), doi: 10.1130/0091-7613(1987)15<614:UTLTMT>2.0.CO;2.

Furtney, M. (2016), Using a multi-sensor satellite perspective for global volcano monitoring, M.S. thesis, Cornell University, Ithaca, New York.

Ganci, G., A. Vicari, L. Fortuna, and C. Del Negro (2011), The HOTSAT volcano monitoring system based on combined use of SEVIRI and MODIS multispectral data, *Annals of Geophysics*, 54(5), doi: 10.4401/ag-5338.

Gawarecki, S.J., R.J.P. Lyon, and W. Nordberg (1965), Infrared spectral returns and imagery of the Earth from space and their application to geological problems: Scientific experiments for manned orbital flight, American Astronautical Society, Science and Technology Series, 4, 13-133.

Gillespie, A., Rokugawa, S., Matsunaga, T., Cothorn, J.S., Hook, S., and Kahle, A.B., (1998), A temperature and emissivity separation algorithm for Advanced Spaceborne Thermal Emission and Reflection Radiometer (ASTER) images, IEEE Transactions on Geoscience and Remote Sensing, 36(4), 1113–1126, doi: 10.1109/36.700995.

Global Volcanism Program, (2013), Volcanoes of the World, v. 4.4.3, Venzke, E. (ed.), Smithsonian Institution. Downloaded 26 May 2018, doi: 10.5479/si.GVP.VOTW4-2013.

Global Volcanism Program, (2013). White Island (241040) in Volcanoes of the World, v. 4.5.0. Venzke, E (ed.). Smithsonian Institution. Downloaded 28 Jun 2016 (<http://volcano.si.edu/volcano.cfm?vn=241040>). <http://dx.doi.org/10.5479/si.GVP.VOTW4-2013>.

Goitom, B., Oppenheimer, C., Hammond, J.O.S., Grandin, R., Barnie, T., Donovan, A., Ogubazghi, G., Yohannes, E., Kibrom, G., Kendall, J.-M., Carn, S.A., Fee, D., Sealing, C., Keir, D., et al., (2015), First recorded eruption of Nabro volcano, Eritrea, 2011, Bulletin of Volcanology, 77(10), doi: 10.1007/s00445-015-0966-3.

Grandoni, D., M.L. Battagliere, M.G. Daraio, P. Sacco, A. Coletta, A. Di Federico, and F. Mastracci (2014), Space-based technology for emergency management: The COSMO-SkyMed constellation contribution, Procedia Technology, 16, doi: 10.1016/j.protcy.2014.10.036.

Grapenthin, R., J.T. Freymueller, and S.S. Serovetnikov (2013), Surface deformation of Bezymianny Volcano, Kamchatka, recorded by GPS: The eruptions from 2005 to 2010 and long-term, long-wavelength subsidence, Journal of Volcanology and Geothermal Research, 263, doi: 10.1016/j.jvolgeores.2012.11.012.

Hamling, I.J., C.A. Williams, and S. Hreindsdottir (2016), Depressurization of a hydrothermal system following the August and November 2012 Te Maari eruptions of Tongariro, New Zealand, Geophysical Research Letters, 43, doi: 10.1002/2015GL067264.

Harris, A.J.L., R. Wright, and L.P. Flynn (1999), Remote monitoring of Mount Erebus volcano, Antarctica, using polar orbiters: Progress and prospects, International Journal of Remote Sensing, 20(15-16), 3051-3071, doi: 10.1080/014311699211615.

Harris, A., (2013), *Thermal Remote Sensing of Active Volcanoes: A User's Manual*, Cambridge University Press, New York, in press.

Hautmann, S., Gottsmann, J., Sparks, R.S.J., Mattioli, G.S., Sacks, I.S., and Strutt, M.H., (2010), Effect of mechanical heterogeneity in arc crust on volcano deformation with application to

Soufrière Hills Volcano, Montserrat, West Indies, *Journal of Geophysical Research*, 115(B9), doi: 10.1029/2009JB006909.

Henderson, S.T., and Pritchard, M.E., (2013), Decadal volcanic deformation in the Central Andes Volcanic Zone revealed by InSAR time series, *Geochemistry, Geophysics, Geosystems*, 14(5), 1358–1374, doi: 10.1002/ggge.20074.

Jay, J.A., Welch, M., Pritchard, M.E., Mares, P.J., Mnich, M.E., Melkonian, A.K., Aguilera, F., Naranjo, J.A., Sunagua, M., and Clavero, J., (2013), Volcanic hotspots of the central and southern Andes as seen from space by ASTER and MODVOLC between the years 2000 and 2010, *Geological Society, London, Special Publications*, 380(1), 161–185, doi: 10.1144/SP380.1.

Johnson, D.J. (1992), Dynamics of magma storage in the summit reservoir of Kilauea volcano, Hawaii, *Journal of Geophysical Research*, 97(B2), doi: 10.1029/91JB02839.

Johnson, D.J., Sigmundsson, F., and Delaney, P.T., (2000), Comment on “Volume of magma accumulation or withdrawal estimated from surface uplift or subsidence, with application to the 1960 collapse of Kīlauea volcano” by PT Delaney and DF McTigue, *Bulletin of Volcanology*, 61(7), 491–493, doi: 10.1007/s004450050006.

Krueger, A.J., (1983), Sighting of El Chichon sulfur dioxide clouds with the Nimbus 7 total ozone mapping spectrometer, *Science*, 220(4604), 1377–1379, doi: 10.1126/science.220.4604.1377.

Krueger, A.J., Schaefer, S.J., Krotkov, N., Bluth, G., and Barker, S., (2000), Ultraviolet remote sensing of volcanic emissions, *Remote Sensing of Active Volcanism*, 25–43, doi: 10.1029/GM116p0025.

Krueger, A.J., L.S. Walter, P.K. Bhartia, C.C. Schnetzler, N.A. Krotkov, I. Sprod, and G.J.S. Bluth, (1995), Volcanic sulfur dioxide measurements from the total ozone mapping spectrometer instruments, *Journal of Geophysical Research* 100(D7), 14,057–14,076.

Lara, L.E., (2009), The 2008 eruption of the Chaiten Volcano, Chile: A preliminary report, *Andean Geology*, 36(1), doi: 10.5027/andgeoV36n1-a09.

Lu, Z., (2007), InSAR imaging of volcanic deformation over cloud-prone areas—Aleutian Islands, *Photogrammetric Engineering & Remote Sensing*, 73(3), 245–257, doi: 10.14358/PERS.73.3.245.

Lu, Z., and Dzurisin, D., (2014), *InSAR Imaging of Aleutian Volcanoes*: Springer Berlin Heidelberg, Berlin, Heidelberg, in press.

Malinverni, E.S., D.T. Sandwell, A.N. Tassetti, and L. Cappelletti, (2014), InSAR decorrelation to assess and prevent volcanic risk, *European Journal of Remote Sensing*, 537–556, doi: 10.5721/EuJRS20144730.

Massonnet, D. and K.L. Feigl, (1998), Radar interferometry and its application to changes in the earth's surface, *Reviews of Geophysics*, 36(4), 441-500, doi: 10.1029/97RG03139.

Mastin, L.G., E. Roeloffs, N.M. Beeler, and J.E. Quick (2008), Constraints on the size, overpressure and volatile content of the Mount St. Helens magma system from geodetic and dome-growth measurements during the 2004-2006+ eruption, In: Sherrod, D.R., W.E. Scott, and P.H. Stauffer (eds.), *A Volcano Rekindled: The Renewed Eruption of Mount St. Helens, 2004-2006*, U.S. Geological Survey Professional Paper 1750.

McCormick Kilbride, B., M. Edmonds and J. Biggs (2016), Observing eruptions of gas-rich compressible magmas from space, *Nature Communications*, 7(13744), doi: 10.1038/ncomms13744.

McCormick, B.T., Edmonds, M., Mather, T.A., Campion, R., Hayer, C.S.L., Thomas, H.E., and Carn, S.A., (2013), *Volcano monitoring applications of the Ozone Monitoring Instrument*, Geological Society, London, Special Publications, 380(1), 259–291, doi: 10.1144/SP380.11.

McCormick, B.T., Edmonds, M., Mather, T.A., and Carn, S.A., (2012), First synoptic analysis of volcanic degassing in Papua New Guinea, *Geochemistry, Geophysics, Geosystems*, 13(3), doi: 10.1029/2011GC003945.

McCormick, M.P., L.W. Thomason, and C.R. Trepte, (1995), Atmospheric effects of the Mt. Pinatubo eruption, *Nature*, 373(6513).

McPeters, R.D., P.K. Bhartia, A.J. Krueger, J.R. Herman, C.G. Wellemeyer, C.J. Seftor, G. Jaross, O. Torres, L. Moy, G. Labow, W. Byerly, S.L. Taylor, T. Swissler, and R.P. Cebula (1998), *Earth Probe Total Ozone Mapping Spectrometer (TOMS) data product user's guide*, NASA Technical Publication.

Milillo, P., B. Riel, B. Minchew, S.-H. Yun, M. Simons, and P. Lundgren (2016), On the synergistic use of SAR constellations' data exploitation for earth science and natural hazards response, *IEEE Journal of Selected Topics in Applied Earth Observations and Remote Sensing*, 9(3), doi: 10.1109/JSTARS.2015.2465166.

Moran, S.C., Kwoun, O., Masterlark, T., and Lu, Z., (2006), On the absence of InSAR-detected volcano deformation spanning the 1995–1996 and 1999 eruptions of Shishaldin Volcano, Alaska, *Journal of Volcanology and Geothermal Research*, 150(1-3), 119–131, doi: 10.1016/j.jvolgeores.2005.07.013.

Naranjo, M.F., S.K. Ebmeier, S. Vallejo, P. Ramon, P. Mothes, J. Biggs, and F. Herrera (2016), Mapping and measuring lava volumes from 2002 to 2009 at El Reventador Volcano, Ecuador, from field measurements and satellite remote sensing, *Journal of Applied Volcanology*, 5(8), doi: 10.1186/s13617-016-0048-z.

Nye, C., Keith, T., Eichelberger, J., Miller, T., McNutt, S., Moran, S., Schneider, D., Dehn, J., and Schaefer, J., (2002), The 1999 eruption of Shishaldin Volcano, Alaska: monitoring a distant eruption, *Bulletin of Volcanology*, 64(8), 507–519, doi: 10.1007/s00445-002-0225-2.

Pagli, C., F. Sigmundsson, R. Pederson, P. Einarsson, T. Árnadóttir, and K.L. Feigl (2007), Crustal deformation associated with the 1996 Gjalp subglacial eruption, Iceland: InSAR studies in affected areas adjacent to the Vatnajökull ice cap, *Earth and Planetary Science Letters*, 252(1-2), 24-33, doi: 10.1016/j.epsl.2007.04.019.

Parker, A.L., J. Biggs, R.J. Walters, S.K. Ebmeier, T.J. Wright, N.A. Teanby, and Z. Lu (2015), Systematic assessment of atmospheric uncertainties for InSAR data at volcanic arcs using large-scale atmospheric models: Application to the Cascade volcanoes, United States, *Remote Sensing of Environment*, 170, doi: 10.1016/j.rse.2015.09.003.

Passarelli, L., and Brodsky, E.E., (2012), The correlation between run-up and repose times of volcanic eruptions, *Geophysical Journal International*, 188(3), 1025–1045, doi: 10.1111/j.1365-246X.2011.05298.x.

Patrick, M.R., and Smellie, J.L., (2013), Synthesis: A spaceborne inventory of volcanic activity in Antarctica and southern oceans, 2000–10, *Antarctic Science*, 25(4), 475–500, doi: 10.1017/S0954102013000436.

Pavlonis, M.J., J. Sieglaff, and J.L. Cintineo, (2016) Automated utilization of weather satellites for global mitigation of aviation related volcanic hazards (abstract). In: *Aviation, Range, and Aerospace Meteorology Special Symposium, 5th, and Conference on Environmental Information Processing Techniques, 32nd*, New Orleans, LA, 10-14, January 2016.

Peltier, A., Scott, B., and Hurst, T., (2009), Ground deformation patterns at White Island volcano (New Zealand) between 1967 and 2008 deduced from levelling data: *Journal of Volcanology and Geothermal Research*, 181(3-4), 207–218, doi: 10.1016/j.jvolgeores.2009.01.020.

Pergola, N., F. Marchese, and V. Tramutoli (2004), Automated detection of thermal features of active volcanoes by means of infrared AVHRR records, *Remote Sensing of Environment*, 93(3), doi: 10.1016/j.rse.2004.07.010.

Philibosian, B., and Simons, M., (2011), A survey of volcanic deformation on Java using ALOS PALSAR interferometric time series, *Geochemistry, Geophysics, Geosystems*, 12(11), doi: 10.1029/2011GC003775.

Phillipson, G., Sobradelo, R., and Gottsmann, J., (2013), Global volcanic unrest in the 21st century: An analysis of the first decade: *Journal of Volcanology and Geothermal Research*, 264, 183–196, doi: 10.1016/j.jvolgeores.2013.08.004.

Pieri, D., and M. Abrams, (2004), ASTER watches the world's volcanoes: A new paradigm for volcanological observations from orbit, *Journal of Volcanology and Geothermal Research*, 135(1-2), 13-28, doi: 10.1016/j.jvolgeores.2003.12.018.

Pieri, D., and M. Abrams, (2005), ASTER observations of thermal anomalies preceding the April 2003 eruption of Chikurachki volcano, Kurile Islands, Russia, *Remote Sensing of Environment*, 99(1-2), doi:10.1016/j.rse.2005.06.012.

Pinel, V., A. Hooper, S. De la Cruz-Reyna, G. Reyes-Davila, M.P. Doin, and P. Bascou (2011), The challenging retrieval of the displacement field from InSAR data for andesitic stratovolcanoes: Case study of Popocatepetl and Colima Volcano, Mexico, *Journal of Volcanology and Geothermal Research*, 200(1-2), doi: 10.1016/j.jvolgeores.2010.12.002.

Pinel, V., M.P. Poland, and A. Hooper (2014), Volcanology: Lessons learned from synthetic aperture radar imagery, *Journal of Volcanology and Geothermal Research*, 289, 81-113, doi: 10.1016/j.jvolgeores.2014.10.010.

Potter, S.H., Scott, B.J., Jolly, G.E., Neall, V.E., and Johnston, D.M., (2015), Introducing the Volcanic Unrest Index (VUI): a tool to quantify and communicate the intensity of volcanic unrest: *Bulletin of Volcanology*, 77(9), doi: 10.1007/s00445-015-0957-4.

Prati, C., A. Ferretti, and D. Perissin (2010), Recent advances on surface ground deformation measurement by means of repeated space-borne SAR observations, *Journal of Geodynamics*, 49(3-4), 161-170, doi: 10.1016/j.jog.2009.10.011.

Pritchard, M.E., Henderson, S.T., Jay, J.A., Soler, V., Krzesni, D.A., Button, N.E., Welch, M.D., Semple, A.G., Glass, B., Sunagua, M., Minaya, E., Amigo, A., and Clavero, J., (2014), Reconnaissance earthquake studies at nine volcanic areas of the central Andes with coincident satellite thermal and InSAR observations: *Journal of Volcanology and Geothermal Research*, 280, 90–103, doi: 10.1016/j.jvolgeores.2014.05.004.

Pritchard, M.E., and Simons, M., (2002), A satellite geodetic survey of large-scale deformation of volcanic centres in the central Andes: *Nature*, 418(6894), 167–171, doi: 10.1038/nature00872.

Pritchard, M.E., and Simons, M. (2004), An InSAR-based survey of volcanic deformation in the central Andes, *Geochemistry, Geophysics, Geosystems*, 5(2), doi: 10.1029/2003GC000610.

Pyle, D.M., T.A. Mather, and J. Biggs (2013), Remote sensing of volcanoes and volcanic processes: integrating observation and modelling – introduction, In: Pyle, D.M., T.A. Mather, and J. Biggs (eds), *Remote Sensing of Volcanoes and Volcanic Processes: Integrating Observation and Modelling*, Geological Society, London, Special Publications, 380, doi: 10.1144/SP380.14.

Ramsey, M. (2015), Synergistic use of satellite thermal detection and science: A decadal perspective using ASTER, In: Harris, A.J. T. De Groeve, F. Garel, and S.A. Carn (eds.), *Detecting, Modelling and Responding to Effusive Eruptions*, Geological Society, London, Special Publications, 426, doi: 10.1144/SP426.23.

Ramsey, M., & Dehn, J. (2004), Spaceborne observations of the 2000 Bezymianny, Kamchatka eruption: the integration of high-resolution ASTER data into near real-time monitoring using AVHRR. *Journal of Volcanology and Geothermal Research*, 135(1), 127-146, doi: 10.1016/j.jvolgeores.2003.12.014.

Realmutto, V.J. (1999), The potential use of Earth Observing System data to monitor the passive emission of sulfur dioxide from volcanoes, In: Mougini-Mark, P.J., J.A. Crisp, and J.H. Fink, *Remote Sensing of Active Volcanism*, Geophysical Monograph 116, American Geophysical Union, Washington, D.C., doi: 0.1029/GM116p0101.

Realmutto, V.J., A.J. Sutton, and T. Elias (1997), Multispectral thermal infrared mapping of sulfur dioxide plumes: A case study from the East Rift Zone of Kilauea Volcano, Hawaii, *Journal of Geophysical Research*, 102(B7), doi: 10.1029/96JB03916.

Reath, K.A., M.S. Ramsey, J. Dehn, and P.B. Webley, (2016), Predicting eruptions from precursory activity using remote sensing data hybridization, *Journal of Volcanology and Geothermal Research*, 321, 18-30, doi: 10.1016/j.jvolgeores.2016.04.027.

Rothery, D.A., P.W. Francis, and C.A. Wood, (1988), Volcano monitoring using short wavelength infrared data from satellites, *Journal of Geophysical Research*, 93(B7), doi: 10.1029/JB093iB07p07993.

Salzer, J.T., M. Nikkhoo, T.R. Walter, H. Sudhaus, G. Reyes-Dávila, M. Bretón, and R. Arámbula (2014), Satellite radar data reveal short-term pre-explosive displacements and a complex conduit system at Volcán de Colima, Mexico, *Frontiers in Earth Science*, 2, doi: 10.3389/feart.2014.00012.

Sandwell, D.T., Myer, D., Mellors, R., Shimada, M., Brooks, B., and Foster, J., (2008), Accuracy and Resolution of ALOS Interferometry: Vector Deformation Maps of the Father's Day Intrusion at Kilauea, *IEEE Transactions on Geoscience and Remote Sensing*, 46(11), 3524–3534, doi: 10.1109/TGRS.2008.2000634.

Schwandner, F.M., M.R. Gunson, C.E. Miller, S.A. Carn, A. Elderling, T. Krings, K.R. Verhulst, D.S. Schimel, H.M. Nguyen, D. Crisp, C.W. O'Dell, G.B. Osterman, L.T. Iraci, and J.R. Podolske (2017), Spaceborne detection of localized carbon dioxide sources, *Science*, 358(6360), doi: 10.1126/science.aam5782.

Semple, A.G., M.E. Pritchard, and R.B. Lohman (2017), An incomplete inventory of suspected human-induced surface deformation in North America detected by satellite interferometric synthetic-aperture radar, *Remote Sensing*, 9(12), doi: 10.3390/rs9121296.

Siebert, L., T. Simkin, and P. Kimberly (2010), *Volcanoes of the World: Third Edition*, Smithsonian Institution, in press.

Sigmundsson, F. (2006), *Iceland Geodynamics: Crustal Deformation and Divergent Plate Tectonics*, Springer, Chichester, U. K.

Simons, M., and Rosen, P.A., (2015), Interferometric Synthetic Aperture Radar Geodesy, in *Treatise on Geophysics*, Elsevier, p. 339–385, doi: 10.1016/B978-044452748-6.00059-6.

Stephens, K.J., S.K. Ebmeier, N.K. Young, and J. Biggs (2017), Transient deformation associated with explosive eruption measured at Masaya volcano (Nicaragua) using Interferometric Synthetic Aperture Radar, *Journal of Volcanology and Geothermal Research*, 344, 212-223, doi: 10.1016/j.jvolgeores.2017.05.014

Symonds, R.B., Gerlach, T.M., and Reed, M.H., (2001), Magmatic gas scrubbing: implications for volcano monitoring, *Journal of Volcanology and Geothermal Research*, 108(1), 303–341, doi: 10.1016/S0377-0273(00)00292-4.

Symonds, R.B., W.I. Rose, G.J.S. Bluth and T.M. Gerlach, (1994), Volcanic-gas studies: methods, results, and applications, In: Carroll, M.R. and J.R. Holloway (eds.), *Volatiles in Magmas*, *Reviews in Mineralogy*, v. 30, Mineralogical Society of America, Washington, D.C., doi: 10.2138/rmg.1994.30.1.

Theys, N., R. Champion, L. Clarisse, H. Brenot, J. van Gent, B. Dils, S. Corradini, L. Merucci, P.-F. Coheur, M. Van Roozendael, D. Hurtmans, C. Clerbaux, S. Tait, and F. Ferrucci, (2013), Volcanic SO₂ fluxes derived from satellite data: A survey using OMI, GOME-2, IASI and MODIS, *Atmospheric Chemistry and Physics*, 13(12), 5945-5968, doi: 10.5194/acp-13-5945-2013.

Thomas, H.E. and I.M. Watson (2010), Observations of volcanic emissions from space: current and future perspectives, *Natural Hazards*, 54(2), p. 323-354, doi: 10.1007/s11069-009-9471-3.

Voight, B., Widiwijayanti, C., Mattioli, G., Elsworth, D., Hidayat, D., and Strutt, M., (2010), Magma-sponge hypothesis and stratovolcanoes: Case for a compressible reservoir and quasi-steady deep influx at Soufrière Hills Volcano, Montserrat, *Geophysical Research Letters*, 37(19), doi: 10.1029/2009GL041732.

Watt, S.F.L., D.M. Pyle, and T.A. Mather (2013), Evidence of mid-to-late-Holocene explosive rhyolitic eruptions from Chaiten Volcano, Chile, *Andean Geology*, 40(2), doi: 10.5027/andgeoV40n2-a02.

Wang, T., K. DeGrandpre, Z. Lu, and J.T. Freymueller (2018), Complex surface deformation of Akutan volcano, Alaska revealed from InSAR time series, *International Journal of Applied Earth Observation and Geoinformation*, 64, 171-180, doi: 10.1016/j.jag.2017.09.001.

Wei, M., and Sandwell, D.T., (2010), Decorrelation of L-Band and C-Band Interferometry Over Vegetated Areas in California, *IEEE Transactions on Geoscience and Remote Sensing*, 48(7), 2942–2952, doi: 10.1109/TGRS.2010.2043442.

- Werner, C.A., Doukas, M.P., and Kelly, P.J., (2011), Gas emissions from failed and actual eruptions from Cook Inlet Volcanoes, Alaska, 1989–2006, *Bulletin of Volcanology*, 73(2), 155–173, doi: 10.1007/s00445-011-0453-4.
- Wessel, P., W.H.F. Smith, R. Scharroo, J. Luis, and F. Wobbe (2013), *Generic Mapping Tools: Improved Version Released*, *EOS Transactions*, 94(45), doi: 10.1002/2013EO450001.
- Williams, R.S. and J.D. Friedman (1970), Satellite observations of effusive volcanism, *Journal of the British Interplanetary Society*, 23, 441–450.
- Wright, R., (2016), *MODVOLC: 14 years of autonomous observations of effusive volcanism from space*, Geological Society, London, Special Publications, doi: 10.1144/SP426.12.
- Wright, R., Blackett, M., and Hill-Butler, C., (2015), Some observations regarding the thermal flux from Earth's erupting volcanoes for the period of 2000 to 2014: Satellite observations of volcanic heat, *Geophysical Research Letters*, 42(2), 282–289, doi: 10.1002/2014GL061997.
- Wright, R., and Flynn, L.P., (2004), Space-based estimate of the volcanic heat flux into the atmosphere during 2001 and 2002: *Geology*, 32(3), 189–192, doi: 10.1130/G20239.1.
- Wright, R., Flynn, L., Garbeil, H., Harris, A., and Pilger, E., (2002), Automated volcanic eruption detection using MODIS, *Remote Sensing of Environment*, 82(1), 135–155, doi: 10.1016/S0034-4257(02)00030-5.
- Wright, R., Flynn, L.P., Garbeil, H., Harris, A.J., and Pilger, E., (2004), MODVOLC: near-real-time thermal monitoring of global volcanism: *Journal of Volcanology and Geothermal Research*, 135(1-2), 29–49, doi: 10.1016/j.jvolgeores.2003.12.008.
- Wright, R., and Pilger, E., (2008), Radiant flux from Earth's subaerially erupting volcanoes, *International Journal of Remote Sensing*, 29(22), 6443–6466, doi: 10.1080/01431160802168210.
- Wright, T.J., C. Ebinger, J. Biggs, A. Ayele, G. Yirgu, D. Keir and A. Stork (2006), Magma-maintained rift segmentation at continental rapture in the 2005 Afar dyking episode, *Nature*, 442, 291–294, doi: 10.1038/nature04978.
- Yamaguchi, Y., Kahle, A. B., Tsu, H., Kawakami, T., & Pniel, M. (1998). Overview of advanced spaceborne thermal emission and reflection radiometer (ASTER), *IEEE Transactions on Geoscience and Remote Sensing*, 36(4), 1062–1071, doi: 10.1109/36.700991.
- Yang, K., Krotkov, N.A., Krueger, A.J., Carn, S.A., Bhartia, P.K., and Levelt, P.F., (2007), Retrieval of large volcanic SO₂ columns from the Aura Ozone Monitoring Instrument: Comparison and limitations, *Journal of Geophysical Research*, 112(D24), doi: 10.1029/2007JD008825.
- Zebker, H.A., F. Amelung, and S. Jonsson, (2000), Remote sensing of volcano surface and internal processes using radar interferometry, In: Mouginis-Mark, P.J., J.A. Crisp, and J.H. Fink,

Remote Sensing of Active Volcanism, Geophysical Monograph 116, American Geophysical Union, Washington, D.C., doi: 10.1029/GM116p0179.

ACCEPTED MANUSCRIPT

Highlights

- First global comparison of satellite-detected activity from multiple types of satellite sensors
- Of three types of satellite sensors studied, each contributed unique detections which validates the multi-sensor approach
- Most volcanoes that erupted in the past few decades displayed volcanic activity measurable from satellite
- Satellite sensors detect between 100 and 1000 volcanic activities per year